

Contact-Geometric Dynamics for Dissipative Nonlinear Systems

D.Y. Zhong^{1,2}

¹*State Key Laboratory of Hydroscience and Engineering, Tsinghua University, Beijing 10084, China*

²*Department of Hydraulic Engineering, Tsinghua University, Beijing 10084, China*

Abstract

Dissipative nonlinear waves are ubiquitous in nonequilibrium physical systems, and the Complex Ginzburg-Landau Equation (CGLE) serves as a fundamental model for describing their dynamics. This paper develops a contact-geometric formulation of dissipative field theories, extending the least constraint theorem to complex fields and establishing a link between contact geometry and probability measures. By applying this framework to the 2D CGLE, we derive the dissipative Contact Hamilton-Jacobi (CHJ) equation, which governs the evolution of the action functional. Through canonical transformation and travelling-wave reduction, exact solutions of the CHJ equation are obtained. From a probabilistic perspective, we derive the probability density functional of the 2D CGLE, identify a universal switching line that separates different dynamical regimes, and reveal a first-order periodon–soliton phase transition with a hysteresis loop. The conserved contact potential is identified as the key geometric quantity governing pattern formation in dissipative media, playing a role analogous to

energy in conservative systems. This contact-geometric framework provides a unified analytical tool for studying pattern selection and phase transitions.

Contents

1	Introduction	4
2	Contact Geometric Formulation for Complex Fields	6
2.1	Least Constraint Theorem and Complex Field Extension	6
2.2	Geometry of Probability Measure	11
3	Geometric Dynamics of 2D CGLE	17
3.1	2D Complex Ginzburg-Landau Equation	17
3.2	Contact Dynamics of CGLE	18
3.3	Conservation Laws and Symmetries	19
3.4	Canonical Transformation	21
3.5	Contact Hamilton–Jacobi Equation	24
4	Traveling-Wave Reduction and Analytical Solutions	25
4.1	Travelling-Wave Reduction	25
4.2	Solution of the CHJ Equation	26
4.3	Parameter Closure	27
5	Probabilistic View of Periodon-Soliton State Transitions	30
5.1	Probability Density Function	30
5.2	Normalisation	31
5.3	Probabilistic Perspective of State Transitions	33
5.3.1	Marginal Probability Density for m	33
5.3.2	Switching Line	35
5.3.3	Hysteresis Loop of Periodon–Soliton Transitions	38

6 Concluding Remarks	41
A Solution of Contact Hamilton-Jacobi Equation	42

List of Figures

1 Spatial visualisation of solutions to 2D CGLE based on contact geometry. Column 1 (3D $\text{Re}(W)$, subplots (a), (e), (i), (m)) shows the real part of $W(x, y)$; Column 2 (3D $ W ^2$, subplots (b), (f), (j), (n)) presents the intensity $ W ^2 = J\Phi^2(y)$; Column 3 (2D $\text{Re}(W)$ Contour, subplots (c), (g), (k), (o)) displays the transverse gradient of the real part; Column 4 ($ W ^2$ -arg(W) Overlay, subplots (d), (h), (l), (p)) maps intensity $ W ^2$ to scatter size and phase $\text{arg}(W) = k_x x - \omega t$ to scatter color; Bottom subplots: The left one (subplot (q)) compares shape functions $\phi(y)$ across different m ; the right one (subplot (r)) shows the real/imaginary parts of $W(x, y)$ at the $x = 0$ cross-section, illustrating the transition of solitons from periodicity to localization as $m \rightarrow 1^-$. In the calculations, we set $\mu = 1.0$ and $ k_x = 0.8$	29
--	----

List of Theorems

2.1 Theorem (Least Constraint for Vector Bundles)	6
2.2 Theorem (Least Constraint for Complex Fields)	8
2.1 Lemma (Evolution of Complex Structure under Contact Flow)	11
2.3 Theorem (Probability Measure of Complex Fields from Contact Geometry)	15

List of Tables

1 Travelling-wave parameter.	28
--------------------------------------	----

1 Introduction

Dissipative nonlinear waves represent a typical dynamical behaviour prevalent in nonequilibrium physical systems, with a core characteristic of the system's ability to maintain ordered spatiotemporal structures through the synergistic coupling of external driving, energy dissipation, and nonlinear interactions [1, 2]. This behaviour is distinct from energy-conserving linear waves in conservative systems and also differs from disordered attenuation dominated by pure dissipation [3]. Such wave phenomena permeate multiscale physical scenarios from the macroscopic to the microscopic, including convective patterns in fluid media [4], coherent light propagation in nonlinear optical systems [5], topological excitations in condensed matter systems, and even pattern development in biological tissues [6].

Constructing a unified theoretical framework to analyse their dynamical mechanisms has become a key topic in the fields of nonlinear dynamics and mathematical physics. The Complex Ginzburg-Landau Equation (CGLE) [7], as a foundational model for describing nonequilibrium nonlinear systems, can precisely characterize the balance between driving forces (e.g., thermal buoyancy in convection, gain in optical systems) and dissipation (e.g., viscous dissipation, light absorption), while capturing the phase transition from homogeneous steady states to ordered periodic patterns [8–13]. Its universality makes it a core tool connecting microscopic nonlinear dynamics to macroscopic observable dissipative nonlinear wave phenomena [4, 7, 14, 15].

Despite the CGLE's essential role and broad applicability, research on its nonlinear wave dynamics remains underinvestigated [4, 16–19]. Most existing methods rely on specific analytical techniques or system-specific numerical methods [15, 20, 21]. For instance, some studies tailor approximations for certain parameter regimes (e.g., weak nonlinearity or limited dissipation), while others focus on individual solution types (e.g., periodic waves or solitons) without linking them within a wider framework. This lack of a unified theoretical foundation not only limits the generalisability of conclusions from individual studies but also hinders systematic exploration of how different pattern types develop into one another, a crucial gap emphasising the need for a more cohesive analytical framework [7].

For decades, one of the most significant ideas in the study of dynamics has been the application of geometric methods to analyse complex spatiotemporal dynamics [22, 23]. Many theoretical developments have shown that contact geometry provides a powerful framework for understanding dissipative structures in a unified manner [24–29]. In this paper, we develop a contact-geometric formulation of the CGLE based on our previously reported study on the contact formulation of vector bundles [30], leading to a dissipative contact Hamilton-Jacobi-like equation that governs the evolution of dissipative structures. Our approach extends the classical Hamilton-Jacobi theory to dissipative systems by using contact geometry, which naturally accounts for energy dissipation. This formulation provides a framework for analysing the stability and dynamics of pattern-forming systems.

The main contributions of this work are as follows: (1) we derive a contact geometric formulation of complex wave fields, (2) we establish a dissipative contact Hamilton-Jacobi equation that governs the evolution of the action functional, and (3) we derive the probability measure within the contact-geometric framework, through which we analyse the first-order periodon–soliton phase-transition boundary and hysteresis loop in the contact-CGLE framework. This study not only enhances the theoretical foundation of pattern formation in dissipative systems but also provides a new analytical tool for studying complex spatiotemporal dynamics in various physical and biological systems.

The paper is organised as follows: Section 2 develops the contact geometric formulation of complex fields, extending the Least Constraint Theorem for vector bundles, deriving the contact dynamical equations, and establishing the probability density functional. Section 3 derives the dissipative contact Hamilton-Jacobi (CHJ) equation by generalising classical Hamilton-Jacobi theory to dissipative systems via contact geometry, introducing a canonical transformation to reduce 2D field dynamics to 1D problems, and formulating the equation. Section 4 discusses travelling-wave solutions of the CGLE by reducing the CHJ equation, obtaining its Jacobi elliptic functions, analysing parameter conditions, and demonstrating the transition from periodic waves to solitons as the elliptic modulus approaches unity, supported by detailed spatial distribution visualisations of field properties. Section 5 investigates prob-

abilistic properties of the 2D CGLE, deriving the probability density functional, defining the critical switching line, and exploring the periodon–soliton phase transition and hysteresis. Finally, Section 6 summarises the main contributions and the broader significance of the contact-geometric approach for nonlinear pattern formation in nonequilibrium systems.

2 Contact Geometric Formulation for Complex Fields

2.1 Least Constraint Theorem and Complex Field Extension

Contact geometry is a mathematical framework that can be used to extend classical Hamiltonian mechanics to dissipative systems in which energy is not conserved [28]. Unlike symplectic geometry applied in conservative systems [22], contact geometry employs a contact manifold defined by a contact 1-form Θ that satisfies the non-degeneracy condition $\Theta \wedge (d\Theta)^{\wedge n} \neq 0$. This geometric structure naturally incorporates dissipation by allowing the system to evolve through extremal paths of a constraint function, rather than following conservative energy trajectories.

The core theoretical underpinning of contact geometry for vector bundles is its concluding theorem [30], which formalises the intrinsic contact geometric structure and the extremal evolution of stochastic dissipative systems. It reads:

Theorem 2.1 (Least Constraint for Vector Bundles). *Let $E \subset \mathbb{R}^n$ be an n -dimensional vector space and \mathbb{P} be the space of probability measures about E . The infinite-order stochastic jet bundle $\pi_{E,0}^\infty : J^\infty(E, \mathbb{P}) \rightarrow E$ satisfies the following properties:*

1. *It admits a natural contact manifold (\mathcal{E}, Θ) defined by the contact 1-form*

$$\Theta = dP - \varphi_i dy^i = \mathcal{H} dt - \varphi_i dy^i,$$

where $\mathcal{E} = T^*E \times \mathbb{R}$; $P \in \mathbb{P}$ is the probability measure; $y \in E$, $\varphi_i = B_i^{\mu_1 \dots \mu_\infty} P_{\mu_1 \dots \mu_\infty}$, with $P_{\mu_1 \dots \mu_\infty} = \partial_{\mu_1 \dots \mu_\infty} P$ and $B_i^{\mu_1 \dots \mu_\infty}$ the coefficients, is the probability flux field, such that $(y^i, \varphi_i, t) \in \mathcal{E}$. $\mathcal{H} = dP(y) = y \partial_y P$ is contact probability potential. The volume form $\Theta \wedge (d\Theta)^{\wedge n}$ is non-degenerate, confirming a valid contact structure on $J^\infty(E, \mathbb{P})$.

2. There exists a unique vector field $\mathfrak{X}(\mathcal{E}) = \{X_{\mathcal{H}} \mid X_{\mathcal{H}} \in \ker(d\Theta) \subset T\mathcal{E}\}$ such that:

$$\iota_{X_{\mathcal{H}}}\Theta = -\varepsilon, \quad \iota_{X_{\mathcal{H}}}d\Theta = 0,$$

where $\varepsilon = \varphi_i y^i - dP(\dot{y})$ is a smooth constraint function. The Lie derivative $L_{X_{\mathcal{H}}}\Theta = 0$ ensures the contact structure is preserved along the flow generated by $\mathfrak{X}(\mathcal{E})$.

3. The flow of $\mathfrak{X}(\mathcal{E})$ corresponds to extremal paths of the action of ε , defined as

$$\mathcal{S} = \int \varepsilon dt = - \int \Theta.$$

This implies the system evolves to extremize ε while maximizing the variation of probability P . Moreover, there is a Hamilton-Jacobi-like equation for \mathcal{S} :

$$\frac{\partial \mathcal{S}}{\partial t} + \mathcal{H} \left[y, \frac{\partial S}{\partial y}, t \right] = 0.$$

The above theorem is formulated for real vector bundles of $E \subset \mathbb{R}^n$, but the cases, for example, the systems of CGLE, describe complex amplitude field $W \in \mathbb{C}^n$. It is necessary to extend the contact geometric framework to complex vector fields. For the complex field W and its canonically conjugate field $\Pi^* \in \mathbb{C}^n$ replacing the real local connection φ_i , the contact 1-form Θ (Theorem 2.1, Property 1) is generalized to account for complex conjugacy. As a result, the extended contact manifold $\mathcal{E}_{\mathbb{C}} = T^*E_{\mathbb{C}} \times \mathbb{R}$ with coordinates (W^j, Π_j^*, t) , and the contact 1-form:

$$\Theta_{\mathbb{C}} = \mathcal{H}dt - \Pi_j^* dW^j,$$

where \mathcal{H} is the complex contact potential. The non-degeneracy of $\Theta_{\mathbb{C}} \wedge (d\Theta_{\mathbb{C}})^{\wedge n}$ is preserved, as dW^j and $d\Pi_j^*$ are linearly independent complex differentials.

The real constraint function ε (Theorem 2.1, Property 2) is extended to complex fields by enforcing hermiticity. The complex constraint function is:

$$\varepsilon_{\mathbb{C}} = \Pi_j^* \dot{W}^j - \mathcal{H}.$$

Using the extended contact structure $\Theta_{\mathbb{C}}$ and constraint $\varepsilon_{\mathbb{C}}$, the contact dynamical equations (Theorem 2.1, Property 3) are derived via the Poisson bracket generalized to complex

functionals. For the complex field W and its conjugate Π^* :

$$\left\{ \begin{array}{l} \frac{\partial W^j}{\partial t} = \{W^j, \mathcal{H}\} = \frac{\partial \mathcal{H}}{\partial \Pi_j^*}, \\ \frac{\partial \Pi_j^*}{\partial t} = \{\Pi_j^*, \mathcal{H}\} = -\frac{\partial \mathcal{H}}{\partial W^j}, \end{array} \right. \quad (2.1a)$$

$$\left\{ \begin{array}{l} \frac{\partial \varepsilon_{\mathbb{C}}}{\partial t} = -\{\varepsilon_{\mathbb{C}}, \mathcal{H}\}. \end{array} \right. \quad (2.1b)$$

$$\left\{ \begin{array}{l} \frac{\partial \varepsilon_{\mathbb{C}}}{\partial t} = -\{\varepsilon_{\mathbb{C}}, \mathcal{H}\}. \end{array} \right. \quad (2.1c)$$

For any two functionals $F(W, \Pi^*)$ and $G(W, \Pi^*)$, the Poisson bracket in equation (2.6) is defined as:

$$\{F, G\} = \frac{\partial F}{\partial W^j} \frac{\partial G}{\partial \Pi_j^*} - \frac{\partial F}{\partial \Pi_j^*} \frac{\partial G}{\partial W^j}. \quad (2.2)$$

The complex field W and its canonically conjugate local connection Π^* form a pair of conjugate variables. Thus,

$$\{W^i, \Pi_j^*\} = \delta_j^i, \quad (2.3)$$

where δ is the Dirac delta function. All other fundamental brackets vanish:

$$\left\{ \begin{array}{l} \{W^i, W^i\} = 0, \\ \{\Pi_i^*, \Pi_i^*\} = 0. \end{array} \right. \quad (2.4a)$$

$$\left\{ \begin{array}{l} \{W^i, W^i\} = 0, \\ \{\Pi_i^*, \Pi_i^*\} = 0. \end{array} \right. \quad (2.4b)$$

With the bracket defined above, the time evolution of any functional $F(W, \Pi^*)$ is given by:

$$\frac{dF}{dt} = \{F, \mathcal{H}\} + \frac{\partial F}{\partial t}. \quad (2.5)$$

The above extension can be summarised as the following theorem:

Theorem 2.2 (Least Constraint for Complex Fields). *Let $E_{\mathbb{C}}$ be an infinite-dimensional function space with values in \mathbb{C}^n , and let \mathbb{P} be the space of probability measures. The infinite-order stochastic jet bundle $\pi_{E_{\mathbb{C}}, 0}^{\infty} : J^{\infty}(E_{\mathbb{C}}, \mathbb{P}) \rightarrow E_{\mathbb{C}}$ satisfies the following properties:*

(1) **Contact manifold structure:** *There exists a natural contact manifold $(\mathcal{E}_{\mathbb{C}}, \Theta_{\mathbb{C}})$ on $J^{\infty}(E_{\mathbb{C}}, \mathbb{P})$, defined by the contact 1-form*

$$\Theta_{\mathbb{C}} = \mathcal{H} dt - \Pi_j^*(\mathbf{r}, t) dW^j(\mathbf{r}, t),$$

where

- (a) $\mathcal{E}_{\mathbb{C}} = T^*E_{\mathbb{C}} \times \mathbb{R}$ is extended complex phase space,
- (b) $W^j(\mathbf{r}, t)$ is the complex field as a section of the complex vector bundle,
- (c) $\Pi_j^*(\mathbf{r}, t) = B_j^{\mu_1 \dots \mu_\infty} P_{\mu_1 \dots \mu_\infty}$ is canonically conjugate field of W^j , and $P_{\mu_1 \dots \mu_k} = \partial_{\mu_1 \dots \mu_k} P$ ($k = 1, \dots, \infty$),
- (d) $\mathcal{H} = \mathcal{H}[W, \Pi^*, t]$ is the complex contact potential.

The corresponding contact volume form is defined within the field-theoretic framework as:

$$\Omega_{\mathbb{C}} = \Theta_{\mathbb{C}} \wedge (d\Theta_{\mathbb{C}})^{\wedge n},$$

where

$$n = \frac{1}{2} \operatorname{rank} (d\Theta_{\mathbb{C}}|_{\ker \Theta_{\mathbb{C}}})$$

is half the dimension of the transverse symplectic structure of the contact form.

- (2) **Unique vector field:** There exists a unique vector field $\mathfrak{X}(\mathcal{E}_{\mathbb{C}}) = \{X_{\mathcal{H}} \mid X_{\mathcal{H}} \in \ker(d\Theta_{\mathbb{C}}) \subset T\mathcal{E}_{\mathbb{C}}\}$ such that

$$\iota_{X_{\mathcal{H}}} \Theta_{\mathbb{C}} = -\varepsilon_{\mathbb{C}}, \quad \iota_{X_{\mathcal{H}}} d\Theta_{\mathbb{C}} = 0,$$

where $\varepsilon_{\mathbb{C}} = \Pi_j^* \dot{W}^j - \mathcal{H}$ is a smooth complex constraint functional and satisfied that $d\varepsilon_{\mathbb{C}} = 0$. The Lie derivative $L_{X_{\mathcal{H}}} \Theta_{\mathbb{C}} = 0$ guarantees that the contact structure is preserved along the flow generated by $\mathfrak{X}(\mathcal{E}_{\mathbb{C}})$.

- (3) **Extremal paths and the contact Hamilton–Jacobi equation:** The flow of $\mathfrak{X}(\mathcal{E}_{\mathbb{C}})$ corresponds to the extremal paths of the action functional of $\varepsilon_{\mathbb{C}}$, defined as

$$\mathcal{S} = \int \varepsilon_{\mathbb{C}} dt = - \int \Theta_{\mathbb{C}}.$$

This implies that the system evolves to extremize $\varepsilon_{\mathbb{C}}$ while maximizing the variation of the probability functional P . There exists a contact Hamilton–Jacobi-type equation:

$$\frac{\partial \mathcal{S}}{\partial t} + \mathcal{H} \left[W, \frac{\partial \mathcal{S}}{\partial W}, t \right] = 0,$$

where $\partial\mathcal{S}/\partial W = \Pi^*$. Moreover, $d\mathcal{S} = 0$ results in dynamical equations:

$$\begin{cases} \frac{\partial W}{\partial t} = \{W, \mathcal{H}\}, \end{cases} \quad (2.6a)$$

$$\begin{cases} \frac{\partial \Pi^*}{\partial t} = \{\Pi^*, \mathcal{H}\}, \end{cases} \quad (2.6b)$$

$$\begin{cases} \frac{\partial \varepsilon_{\mathbb{C}}}{\partial t} = -\{\varepsilon_{\mathbb{C}}, \mathcal{H}\}. \end{cases} \quad (2.6c)$$

Proof. Details are the same as those of Theorem 2.1 as reported in [30], with the extension to complex vector bundles. The key extension steps are outlined as follows:

Step 1: Complex Vector Bundle Setup: Define the complex vector space $E_{\mathbb{C}}$ and its associated infinite-order stochastic jet bundle $J^\infty(E_{\mathbb{C}}, \mathbb{P})$, replacing the real vector space E in the original theorem with complex-valued fields $W \in E_{\mathbb{C}} \subset \mathbb{C}^n$ and their canonically conjugate fields $\Pi^* \in T^*E_{\mathbb{C}}$.

Step 2: Complex Contact Manifold Construction: Generalize the real contact 1-form to the complex case

$$\Theta_{\mathbb{C}} = \mathcal{H}dt - \Pi_j^* dW^j,$$

Verify the non-degeneracy of the contact volume form

$$\Omega_{\mathbb{C}} = \Theta_{\mathbb{C}} \wedge (d\Theta_{\mathbb{C}})^{\wedge n}$$

by leveraging linear independence of dW^j and $d\Pi_j^*$.

Step 3: Unique Vector Field Extension: Extend the real vector field $\mathfrak{X}(E)$ to $\mathfrak{X}(E_{\mathbb{C}}) \subset \ker(d\Theta_{\mathbb{C}})$

$$\varepsilon_{\mathbb{C}} = \Pi_j^* \dot{W}^j - \mathcal{H}.$$

Confirm the conditions $\iota_{X_{\mathcal{H}}} \Theta_{\mathbb{C}} = -\varepsilon_{\mathbb{C}}$ and $\iota_{X_{\mathcal{H}}} d\Theta_{\mathbb{C}} = 0$, and preserve the contact structure via $L_{X_{\mathcal{H}}} \Theta_{\mathbb{C}} = 0$.

Step 4: Complex Poisson Bracket and Dynamical Equations: Generalize the real Poisson bracket to complex functionals $F(W, \Pi^*)$ and $G(W, \Pi^*)$ as

$$\{F, G\} = \frac{\partial F}{\partial W^j} \frac{\partial G}{\partial \Pi_j^*} - \frac{\partial F}{\partial \Pi_j^*} \frac{\partial G}{\partial W^j},$$

derive the complex contact dynamical equations Eq. (2.6), and ensure consistency with the conjugate variable relation $\{W^i, \Pi_j^*\} = \delta_j^i$.

Step 5: Extremal Paths and CHJ Equation: Extend the real action functional \mathcal{S} to the complex case

$$\mathcal{S} = \int \varepsilon_C dt = - \int \Theta_C,$$

establish the relation $\partial \mathcal{S} / \partial W^j = \Pi_j^*$, and derive the contact Hamilton-Jacobi equation by extremizing \mathcal{S} while maximizing the probability variation dP :

$$\frac{\partial \mathcal{S}}{\partial t} + \mathcal{H} \left[W^j, \frac{\partial \mathcal{S}}{\partial W^j}, t \right] = 0.$$

□

2.2 Geometry of Probability Measure

Within the contact-geometric framework developed in this work, the probability measure $P[W]$ plays a fundamental role in characterising the statistical properties of dissipative structures. This subsection derives the explicit form of $P[W]$ and provides its geometric interpretation.

Lemma 2.1 (Evolution of Complex Structure under Contact Flow). *Let (\mathcal{E}, Θ) be a complex contact manifold of complex dimension $2n + 1$ with contact distribution $\ker \Theta$ and induced symplectic form $\omega = d\Theta|_{\ker \Theta}$. Let $X \in \mathfrak{X}(\mathcal{E})$ be the unique characteristic vector field satisfying*

$$L_X \Theta = 0, \quad \iota_X \Theta = -\varepsilon, \quad \iota_X \omega = 0, \quad d\varepsilon(X) = 0.$$

Let J be an ω -compatible complex structure on $\ker \Theta$. Define the intrinsic symplectic volume as follows. At each point $p \in \mathcal{E}$, choose a symplectic frame $\{e_i, \tilde{e}_i\}_{i=1}^n \subset \ker \Theta$ satisfying

$$\tilde{e}_i = Je_i, \quad \omega(e_i, \tilde{e}_j) = \delta_{ij}, \quad \omega(e_i, e_j) = \omega(\tilde{e}_i, \tilde{e}_j) = 0.$$

Define

$$\mathcal{V}_{\text{int}} = \text{Re}[\omega^{\wedge n}(e_1, \tilde{e}_1, \dots, e_n, \tilde{e}_n)] \neq 0.$$

Then the Lie derivative of J along X must satisfy

$$L_X J = -\varepsilon J,$$

and consequently,

$$L_X \mathcal{V}_{\text{int}} = -n\varepsilon \mathcal{V}_{\text{int}}.$$

Proof. **Step 1: Flow extension of symplectic frame.** Let ϕ_t be the flow generated by the vector X . Fix $p_0 \in \mathcal{E}$ and a symplectic frame $\{e_i(0), \tilde{e}_i(0)\}$ at p_0 satisfying the given conditions. Extend the frame along the integral curve $p_t = \phi_t(p_0)$ by push-forward ϕ_{t*} and transformation $J(p_t)$, respectively:

$$e_i(t) = \phi_{t*} e_i(0), \quad \tilde{e}_i(t) = J(p_t) e_i(t).$$

Define the pairing matrix $A(t) = (A_{ij}(t))$ with $A_{ij}(t) = \omega(e_i(t), \tilde{e}_j(t))$. Since $A(0) = I_n$, we have $\det A(0) = 1$.

Step 2: Invariance under flow.

Noticing that $(\phi_t^* J)(p_0) e_j(0) = \phi_{t*}^{-1} [J(p_t)(\phi_{t*} e_j(0))]$, we had that

$$\phi_{t*}(\phi_t^* J)(p_0) e_j(0) = \phi_{t*} \phi_{t*}^{-1} [J(p_t)(\phi_{t*} e_j(0))] = J(p_t)(\phi_{t*} e_j(0)),$$

then using $L_X \omega = 0$ (from $L_X \Theta = 0$ and $\omega = d\Theta|_{\ker \Theta}$), we express:

$$A_{ij}(t) = \omega(\phi_{t*} e_i(0), J(p_t) \phi_{t*} e_j(0)) = \omega(e_i(0), (\phi_t^* J)(p_0) e_j(0)).$$

Let $J(t) = \phi_t^* J$ (pullback of J) and $F(t) = \det A(t)$. Note that $F(t) = \det A(t)$ and $A(t)$ is the pairing matrix defined on the contact flow ϕ_t (i.e., on the points of the integral curve $p_t = \phi_t(p_0)$), so $F(t)$ is also a scalar quantity associated with $\phi(t)$. Then $\mathcal{V}_{\text{int}} = \text{Re}[F(t)]$ (up to constant factor).

Step 3: Evolution of complex structure. Differentiate $A(t)$ at $t = 0$:

$$\dot{A}_{ij}(0) = \omega(e_i(0), \dot{J}(0) e_j(0)), \quad \dot{J}(0) = L_X J.$$

Consider the Hermitian metric $h(U, V) = \omega(U, JV)$. Compute:

$$L_X h(U, V) = (L_X \omega)(U, JV) + \omega(U, (L_X J)V) = \omega(U, (L_X J)V),$$

since $L_X\omega = 0$. For h to remain Hermitian, $L_Xh = \lambda h$ for some λ , implying $L_XJ = \lambda J$.

To determine λ , use the contact condition $\iota_X\Theta = -\varepsilon$ and $X(\varepsilon) = 0$ (so ε is constant). The contact form Θ induces $\omega = d\Theta|_{\ker\Theta}$, and the flow of X scales Θ by $-\varepsilon$ (since $\iota_X\Theta = -\varepsilon$). As J is ω -compatible, its evolution must match this scaling:

$$L_XJ = -\varepsilon J. \quad (2.7)$$

Step 4: Volume evolution.

To establish the key identity linking the time derivative of the pullback of the complex structure J to the pullback of its Lie derivative along the characteristic vector field X , we proceed as follows:

Let $\phi_t : E \rightarrow E$ denote the one-parameter diffeomorphism group (flow) generated by X , satisfying the group operation $\phi_{t+s} = \phi_t \circ \phi_s$ for all $t, s \in \mathbb{R}$. By the composition law of pullback operations for diffeomorphisms, we have $(\phi_t \circ \phi_s)^*J = \phi_s^*(\phi_t^*J)$, which simplifies to $\phi_{t+s}^*J = \phi_s^*(\phi_t^*J)$ due to the group structure.

Next, we define the time derivative of the pullback tensor field ϕ_t^*J . For a fixed t , the derivative with respect to t is given by the limit of the difference quotient as $s \rightarrow 0$, i.e.,

$$\frac{d}{dt}(\phi_t^*J) = \frac{d}{ds} \bigg|_{s=0} \phi_{t+s}^*J.$$

This expression captures the instantaneous rate of change of ϕ_t^*J along the flow generated by X .

Substituting the group property $\phi_{t+s}^*J = \phi_s^*(\phi_t^*J)$ into the derivative definition, we rewrite the right-hand side as

$$\frac{d}{dt}(\phi_t^*J) = \frac{d}{ds} \bigg|_{s=0} \phi_s^*(\phi_t^*J).$$

Recall the flow-based definition of the Lie derivative: for any tensor field T , the Lie derivative along X is $\mathcal{L}_X T = \frac{d}{ds} \bigg|_{s=0} \phi_s^*T$. Identifying $T = \phi_t^*J$ in this definition, the right-hand side of the above equation is exactly $\mathcal{L}_X(\phi_t^*J)$, leading to

$$\frac{d}{dt}(\phi_t^*J) = \mathcal{L}_X(\phi_t^*J).$$

We now invoke the commutativity between pullback and Lie derivative for the flow ϕ_t generated by X : for any diffeomorphism ϕ_s in the group and any tensor field T , the pullback preserves the Lie derivative, i.e., $\phi_s^*(\mathcal{L}_X T) = \mathcal{L}_X(\phi_s^* T)$. Setting $s = t$ and $T = J$, this commutativity yields $\mathcal{L}_X(\phi_t^* J) = \phi_t^*(\mathcal{L}_X J)$.

Combining the two results above, we arrive at the desired identity:

$$\frac{d}{dt}(\phi_t^* J) = \phi_t^*(\mathcal{L}_X J).$$

The flow ϕ_t of X scales the complex structure exponentially:

$$\phi_t^* J = e^{-\int \varepsilon dt} J.$$

Recall the definition $A_{ij}(t) = \omega(e_i(t), Je_j(t))$ with the frame $e_i(t) = \phi_{t*}e_i(0)$. Using the invariance $L_X\omega = 0$ (which follows from $L_X\Theta = 0$ and $\omega = d\Theta|_{\ker\Theta}$) we obtain

$$\begin{aligned} A_{ij}(t) &= \omega(\phi_{t*}e_i(0), J(p_t) \phi_{t*}e_j(0)) \\ &= \omega(e_i(0), (\phi_t^* J)(p_0) e_j(0)) \\ &= e^{-\varepsilon t} \omega(e_i(0), J(p_0) e_j(0)). \end{aligned}$$

At $t = 0$ the frame was chosen so that $\omega(e_i(0), Je_j(0)) = \delta_{ij}$; therefore

$$A(t) = e^{-\int \varepsilon dt} I_n.$$

Consequently,

$$F(t) = \det A(t) = e^{-n \int \varepsilon dt},$$

and its derivative is

$$\dot{F}(t) = -n\varepsilon e^{-n \int \varepsilon dt} = -n\varepsilon F(t). \quad (2.8)$$

Evaluating at $t = 0$ gives $\dot{F}(0) = -n\varepsilon$, which is consistent with the computation via Jacobi's formula. Since (2.8) holds for every t , the Lie derivative of F satisfies

$$L_X F = -n\varepsilon F. \quad (2.9)$$

Finally, the intrinsic symplectic volume is defined as $\mathcal{V}_{\text{int}} = \text{Re}[F]$ (up to a constant factor). Because ε is real, taking the real part commutes with the Lie derivative, yielding

$$L_X \mathcal{V}_{\text{int}} = \text{Re}[L_X F] = \text{Re}[-n\varepsilon F] = -n\varepsilon \text{Re}[F] = -n\varepsilon \mathcal{V}_{\text{int}}. \quad (2.10)$$

Step 5: Normalization independence. If $\omega(e_i, \tilde{e}_j) = c\delta_{ij}$, then $F(0) = c^n$ and $\dot{F}(0) = -n\varepsilon c^n$, so the evolution equation holds for any frame normalization. \square

Theorem 2.3 (Probability Measure of Complex Fields from Contact Geometry). *In the setting of Theorem 2.2, consider the contact manifold $(\mathcal{E}_{\mathbb{C}}, \Theta_{\mathbb{C}})$, the contact volume form $\Omega_{\mathbb{C}} = \Theta_{\mathbb{C}} \wedge (d\Theta_{\mathbb{C}})^{\wedge n}$, the unique vector field $X_{\mathcal{H}}$, and the action functional $\mathcal{S} = -\int \Theta_{\mathbb{C}}$. Let $\pi : \mathcal{E}_{\mathbb{C}} \rightarrow E_{\mathbb{C}}$ be the projection $\pi(t, W, \Pi^*) = W$. Then, there exists a probability density functional on space $E_{\mathbb{C}}$ of the form*

$$\mathcal{P}[W] = \frac{1}{\mathcal{Z}} \exp(\mathcal{S}[W]), \quad \mathcal{Z} = \int_{E_{\mathbb{C}}} \exp(\mathcal{S}[W]) \mathcal{D}W,$$

where $\mathcal{S}[W] = -\int \Theta_{\mathbb{C}}$ is the action functional defined in Theorem 2.2, and $\mathcal{D}W$ denotes the formal volume element on $E_{\mathbb{C}}$.

Proof. We proceed through the following geometrically motivated steps.

Step 1: Finite-dimensional approximation of the contact structure. Consider a complex contact manifolds $(\mathcal{E}_{\mathbb{C}}, \Theta_{\mathbb{C}})$ with $\dim_{\mathbb{C}} \mathcal{E}_{\mathbb{C}} = 2n + 1$, where

$$n = \frac{1}{2} \operatorname{rank}_{\mathbb{C}}(d\Theta_{\mathbb{C}}|_{\operatorname{Ker} \Theta_{\mathbb{C}}}).$$

Each manifold satisfies the non-degeneracy condition

$$\Theta_{\mathbb{C}} \wedge d\Theta_{\mathbb{C}}^{\wedge n} \neq 0,$$

and carries the induced symplectic form on the contact distribution:

$$\omega_{\mathbb{C}} = d\Theta_{\mathbb{C}}|_{\operatorname{Ker} \Theta_{\mathbb{C}}}.$$

By Theorem 2.2, there exists a unique vector field $X_{\mathcal{H}}$ satisfying

$$\iota_{X_{\mathcal{H}}} \Theta_{\mathbb{C}} = -\varepsilon_{\mathbb{C}}, \quad \iota_{X_{\mathcal{H}}} \omega_{\mathbb{C}} = 0,$$

where $\varepsilon_{\mathbb{C}} = \partial_t \mathcal{S}$ and $\mathcal{S} = -\int \Theta_{\mathbb{C}}$ is the action functional. Let $\pi : \mathcal{E}_{\mathbb{C}} \rightarrow E_{\mathbb{C}}$ denote the canonical projection.

Step 2: Intrinsic symplectic volume evolution. On contact distribution $\text{Ker } \Theta_{\mathbb{C}}$, choose a symplectic frame $\{e_1, Je_1, \dots, e_n, Je_n\}$ as in the Lemma, and define the intrinsic symplectic volume

$$\mathcal{V}_{\text{int}} = \text{Re}[(\omega_{\mathbb{C}})^{\wedge n}(e_1, Je_1, \dots, e_n, Je_n)] \neq 0. \quad (2.11)$$

According to Lemma 2.1, the Lie derivative of \mathcal{V}_{int} along $X_{\mathcal{H}}$ satisfies

$$\mathcal{L}_{X_{\mathcal{H}}} \mathcal{V}_{\text{int}} = -n \varepsilon_{\mathbb{C}} \mathcal{V}_{\text{int}}. \quad (2.12)$$

Step 3: Construction of an invariant measure along the characteristic flow. From the evolution equation (2.12), we obtain

$$\begin{aligned} \mathcal{V}_{\text{int}}(t) &= \mathcal{V}_{\text{int}}(0) \exp\left(-n \int_0^t \varepsilon_{\mathbb{C}}(s) \, ds\right) \\ &= \mathcal{V}_{\text{int}}(0) \exp\left(-n(\mathcal{S}(t) - \mathcal{S}(0))\right). \end{aligned}$$

Consequently,

$$\mathcal{I} = \mathcal{V}_{\text{int}}(t) \exp(n\mathcal{S}(t)) = \mathcal{V}_{\text{int}}(0) \exp(n\mathcal{S}(0)). \quad (2.13)$$

This shows that the quantity \mathcal{I} is constant along the characteristic flow, i.e., $\mathcal{L}_{X_{\mathcal{H}}} \mathcal{I} = 0$. Therefore, we can define the measure μ as

$$\mu dt = \exp(n\mathcal{S}(t, W)) \mathcal{V}_{\text{int}}(t) dt \wedge d^{\wedge n}W = \mathcal{I} dt \wedge d^{\wedge n}W. \quad (2.14)$$

Step 4: Pushforward to the configuration space and emergence of the probability density. We now push forward the measure μ to the configuration space $E_{\mathbb{C}}$. The projection $\pi : \mathcal{E}_{\mathbb{C}} \rightarrow E_{\mathbb{C}}$ sends (W, Π^*) to W . For a measurable set A in $E_{\mathbb{C}}$, we have

$$((\pi)_* \mu)(A) = \int_{\pi^{-1}(A)} \mu = \int_A \mathcal{I} d^nW. \quad (2.15)$$

Thus, we define a probability measure on $E_{\mathbb{C}}$ by

$$dP(W) = \frac{1}{Z} \mathcal{I} d^nW, \quad Z = \int_{E_{\mathbb{C}}} \mathcal{I} d^nW. \quad (2.16)$$

Here we assume $Z < \infty$, i.e., the measure is normalizable.

□

3 Geometric Dynamics of 2D CGLE

3.1 2D Complex Ginzburg-Landau Equation

In this paper, we study the 2-dimensional Complex Ginzburg-Landau Equation (CGLE) for studying dispersive waves [4, 31, 32] given by

$$\frac{\partial W}{\partial t} = \mu W - |W|^2 W + \left(\partial_x - \frac{i}{2} \partial_y^2 \right)^2 W, \quad (3.1)$$

where we use ∂_x and ∂_x stand for, respectively, $\frac{\partial}{\partial x}$ and $\frac{\partial}{\partial y}$.

To understand the essential nature of the CGLE, we define a 2D differential operator \mathcal{L} as:

$$\mathcal{L} = \partial_x - \frac{i}{2} \partial_y^2. \quad (3.2)$$

For complex functions $f, g \in \mathbb{C}^\infty$ decaying at infinity, the adjoint \mathcal{L}^\dagger is defined by:

$$\langle f, \mathcal{L}g \rangle \equiv \iint f^*(\mathcal{L}g) dx dy = \iint (\mathcal{L}^\dagger f)^* g dx dy.$$

Through integration by parts and by vanishing conditions of boundary terms, we had that

$$\langle f, \mathcal{L}g \rangle = \iint \left[(\partial_x f)^* - \left(-\frac{i}{2} \right)^* (\partial_y^2 f)^* \right] g dx dy.$$

Since $\left(-\frac{i}{2} \right)^* = \frac{i}{2}$, this leads to define that:

$$\mathcal{L}^\dagger = -\partial_x + \frac{i}{2} \partial_y^2, \quad (3.3)$$

confirming the skew-adjoint property $\mathcal{L}^\dagger = -\mathcal{L}$.

The skew-adjoint property $\mathcal{L}^\dagger = -\mathcal{L}$ plays a pivotal role in the dynamics of the CGLE and the study of dispersive waves. First, it imposes a rigid constraint on the spectrum of \mathcal{L} , ensuring all eigenvalues are purely imaginary—this directly translates to the oscillatory and nondissipative propagation of dispersive wave modes, as the linear evolution generated by \mathcal{L} (and its square \mathcal{L}^2 in the CGLE) avoids exponential growth or decay inherent to dissipative/amplifying systems. Second, the skew-adjointness guarantees that $\mathcal{L}^2 = -\mathcal{L}^\dagger \mathcal{L}$ is a self-adjoint operator, whose real spectrum underpins the well-posedness of the CGLE's

linearization and simplifies the decomposition of dispersive wave modes. Third, this property preserves the conservative nature of the dispersive term in the equation, distinguishing it from the nonlinear ($|W|^2W$) and gain/loss (μW) terms, thereby providing a mathematical foundation for analyzing the stability, periodicity, and propagation characteristics of dispersive waves described by the CGLE.

3.2 Contact Dynamics of CGLE

In the above equations, \mathcal{H} can be determined by

$$\varepsilon_{\mathbb{C}} = \Pi^* \dot{W} - \mathcal{H}, \quad \dot{W} = \partial \mathcal{H} / \partial \Pi^* \quad \Rightarrow \quad \varepsilon_{\mathbb{C}} = \Pi^* \frac{\partial \mathcal{H}}{\partial \Pi^*} - \mathcal{H},$$

with the solution [30]:

$$\mathcal{H}[W, \Pi^*, t] = \mathcal{H}_{\text{par}}[W, \Pi^*, t] + \mathcal{H}_{\text{hom}}[W, \Pi^*, t], \quad (3.4)$$

of which

$$\mathcal{H}_{\text{hom}}[W, \lambda \Pi^*, t] = \lambda \mathcal{H}_{\text{hom}}[W, \Pi^*, t]$$

for $\lambda \neq 0$.

In the contact-geometric framework, the component \mathcal{H}_{par} imposes constraints not only on the geometry of the configuration space. With \mathcal{H}_{par} explicitly incorporated into the dynamical equations, they can, in principle, yield direct solutions tailored to the prescribed configuration, boundary, and initial conditions. However, retaining \mathcal{H}_{par} in the equations substantially complicates their solution.

To simplify the analysis while preserving the non-degeneracy of the contact structure, we impose the constraint function to be a non-zero constant C , corresponding to $\mathcal{H}_{\text{par}} = C$. This yields the constraint $\varepsilon_{\mathbb{C}} = -C \neq 0$, ensuring the contact form remains non-degenerate. However, this choice corresponds to a trivial particular solution—a constant solution, which does not contribute to the essential dynamics of the system. Since constant terms do not affect the Poisson bracket structure, the equations of motion are completely generated by the homogeneous part \mathcal{H}_{hom} .

In line with standard practice in dynamical system analysis, we therefore derive the general solutions using the homogeneous contact potential \mathcal{H}_{hom} and subsequently impose the relevant constraints. This approach yields the same dynamical equations as setting $\mathcal{H}_{\text{par}} = 0$ but avoids the theoretical issue of contact form degeneracy, allowing us to focus on the non-trivial dynamics of the system.

Thus:

$$\mathcal{H} = -(\mathcal{L}W)(\mathcal{L}\Pi^*) + \mu W\Pi^* - |W|^2W\Pi^*. \quad (3.5)$$

In fact, we had that

$$\begin{aligned} \mathcal{H} &= \Pi^* \mathcal{L}^2 W + \mu W\Pi^* - |W|^2 W\Pi^* \\ &= \Pi^* [\mathcal{L}^2 W + \mu W - |W|^2 W] \\ &= \Pi^* \dot{W}. \end{aligned}$$

Clearly, $\mathcal{H}(W, \lambda\Pi^*) = \lambda\mathcal{H}(W, \Pi^*)$, and thus it is homogeneous solution as required.

Using the Poisson bracket definition and functional derivatives:

$$\frac{\partial W}{\partial t} = \{W, \mathcal{H}\} = \frac{\partial W}{\partial W} \frac{\partial \mathcal{H}}{\partial \Pi^*} - \frac{\partial W}{\partial \Pi^*} \frac{\partial \mathcal{H}}{\partial W} = \frac{\partial \mathcal{H}}{\partial \Pi^*(\mathbf{r})}. \quad (3.6)$$

We compute the functional derivatives of the contact potential:

$$\begin{aligned} \dot{W} &= \frac{\partial \mathcal{H}}{\partial \Pi^*} = \frac{\partial}{\partial \Pi^*} [-(\mathcal{L}W)(\mathcal{L}\Pi^*) + \mu W\Pi^* - |W|^2W\Pi^*] \\ &= \mathcal{L}^2 W + \mu W - |W|^2 W, \end{aligned} \quad (3.7)$$

which is exactly the CGLE. Similarly

$$\begin{aligned} \dot{\Pi}^* &= -\frac{\partial \mathcal{H}}{\partial W} = -\frac{\partial}{\partial W} [-(\mathcal{L}W)(\mathcal{L}\Pi^*) + \mu W\Pi^* - |W|^2W\Pi^*] \\ &= -\mathcal{L}^2 \Pi^* - \mu \Pi^* + 2|W|^2 \Pi^*. \end{aligned} \quad (3.8)$$

3.3 Conservation Laws and Symmetries

The contact system possesses the following special quantities:

Contact potential \mathcal{H} . Since \mathcal{H} has no explicit time dependence:

$$\frac{d\mathcal{H}}{dt} = \{\mathcal{H}, \mathcal{H}\} + \frac{\partial\mathcal{H}}{\partial t} = 0.$$

Compared to classical Hamiltonian systems, where the Hamiltonian typically corresponds to physical energy and its conservation is inherently tied to energy conservation, the conservation of the contact potential \mathcal{H} here is a geometric property of the contact manifold structure. This conservation holds universally for the contact dynamical system, independent of whether the system is stable or unstable, distinct from classical Hamiltonian systems where energy conservation is often a direct consequence of time-translation symmetry without explicit geometric constraints.

Energy: $\mathcal{N} = |W|^2$. The Poisson bracket is $\{\mathcal{N}, \mathcal{H}\}$:

$$\begin{aligned} \frac{d\mathcal{N}}{dt} &= \{\mathcal{N}, \mathcal{H}\} = \frac{\partial\mathcal{N}}{\partial W} \frac{\partial\mathcal{H}}{\partial \Pi^*} - \frac{\partial\mathcal{N}}{\partial \Pi^*} \frac{\partial\mathcal{H}}{\partial W} \\ &= W^* \frac{\partial\mathcal{H}}{\partial \Pi^*} - 0 \cdot \frac{\partial\mathcal{H}}{\partial W} \\ &= W^* (\mathcal{L}^2 W + \mu W - |W|^2 W) \\ &= W^* \dot{W}. \end{aligned}$$

This vanishes when systems are in stable states, indicating that the power \mathcal{N} (a quantity analogous to energy in dissipative wave systems) is conserved for stable configurations. For unstable states, however, $\frac{d\mathcal{N}}{dt} \neq 0$, meaning energy is not conserved. This contrasts with classical Hamiltonian systems, where energy conservation is generally maintained regardless of stability (as stability relates to perturbations rather than energy exchange with the environment), while the dissipative nature of the CGLE leads to energy non-conservation in unstable regimes due to unbalanced gain-loss dynamics and nonlinear interactions.

Although energy is not conserved in dissipative systems, the conservation of the contact potential \mathcal{H} provides a powerful new geometric framework for analyzing such systems. Unlike traditional approaches that rely on energy conservation as a fundamental principle, the contact potential's conservation emerges naturally from the contact geometric structure, making it applicable to both stable and unstable states. This geometric conservation law

allows us to systematically study the emergence of ordered structures in dissipative systems, such as the formation of coherent patterns in the CGLE, without being constrained by the limitations of energy conservation. By recognizing this new conserved quantity, we gain a deeper understanding of how dissipative systems maintain their dynamic order through continuous energy exchange with the environment, aligning with the principles of dissipative structure theory where systems maintain stability through continuous energy dissipation rather than energy conservation.

3.4 Canonical Transformation

The Hamilton–Jacobi (HJ) equation is a foundational tool in dynamical systems that connects the action functional to the Hamiltonian and enabling the solution of complex dynamics through action extremisation. For dissipative systems described by contact geometry (Section 2), the classical HJ equation generalises to the contact HJ equation (CHJ), which retains the contact manifold’s geometric structure while accounting for dissipation.

For classical Hamiltonian systems, the HJ equation is derived from the action functional $S[q, t]$ and Hamiltonian $H(q, p, t)$, where q denotes generalised coordinates and $p = \partial S / \partial q$ as canonical momentum. It takes the form:

$$\frac{\partial S}{\partial t} + H\left(q, \frac{\partial S}{\partial q}, t\right) = 0.$$

This equation describes the evolution of the action functional that extremizes the system’s dynamics.

In the contact geometric framework of CGLE, the contact potential $\mathcal{H}[W, \Pi^*, t]$ (Eq. (3.5)) replaces the classical Hamiltonian. The action functional $S[W, t]$ is defined such that the canonical conjugate field $\Pi^*(\mathbf{r}, t)$ to complex field W is the functional derivative of the action:

$$\Pi^*(\mathbf{r}, t) = \frac{\partial S[W, t]}{\partial W(\mathbf{r}, t)}. \quad (3.9)$$

Substituting this relation into the contact dynamical equation for the action functional (2.5),

with no explicit time dependence of \mathcal{H} , we get the CHJ equation for the 2D CGLE:

$$\frac{\partial S}{\partial t} + \mathcal{H} \left[W, \frac{\partial S}{\partial W}, t \right] = 0. \quad (3.10)$$

This is the core equation of this study, which governs the evolution of the action functional $S[W, t]$ in the contact geometric framework.

The direct solution of Eq. (3.10) is challenging due to the complex-valued field $W(\mathbf{r}, t) \in \mathbb{C}$ and 2D functional space. To simplify the equation and enable analytical solutions, we introduce a canonical transformation that maps the complex field W and its conjugate field Π^* to a real-valued field and its corresponding conjugate field, preserving the canonical Poisson bracket structure, which is critical for consistency with contact dynamics.

We define a canonical field transformation that converts the complex scalar field $W(\mathbf{r}, t) \in \mathbb{C}$ and its conjugate connection $\Pi^*(\mathbf{r}, t) \in \mathbb{C}$ to a real field $\Phi(y, t) \in \mathbb{R}$ and its canonical counterpart $\Pi_\Phi(y, t) \in \mathbb{R}$. The transformation is performed at a fixed field intensity J , treated as a time-independent external parameter once the system reaches a statistical steady state such that $\partial J/\partial t = 0$.

We define a type-2 generating functional $F_2[W, \Pi_\Phi, t]$ that depends on the original complex field $W(y, t)$ and the new real conjugate field $\Pi_\Phi(y, t)$:

$$F_2[W, \Pi_\Phi, t] = \sqrt{\frac{2\pi}{J}} \exp(-i(k_x x + \theta(y, t))) W(\mathbf{r}, t) \Pi_\Phi(y, t), \quad (3.11)$$

where $k_x \in \mathbb{R}$ is the fixed wavenumber in the x -direction; $\theta(y, t) \in \mathbb{R}$ is a y -dependent phase ensuring consistency between complex and real descriptions; $J > 0$ is the conserved total intensity $J = \iint_{\mathbb{R}^2} |W(\mathbf{r}, t)|^2 d^2\mathbf{r}$.

The canonical transformation is determined by the functional derivatives of F_2 :

$$\left\{ \begin{array}{l} \Pi^*(\mathbf{r}, t) = \frac{\partial F_2}{\partial W(\mathbf{r}, t)} = \sqrt{\frac{2\pi}{J}} \exp(-i(k_x x + \theta(y, t))) \Pi_\Phi(y, t), \end{array} \right. \quad (3.12a)$$

$$\left\{ \begin{array}{l} \Phi(y, t) = \frac{\partial F_2}{\partial \Pi_\Phi(y, t)} = \sqrt{\frac{2\pi}{J}} \exp(-i(k_x x + \theta(y, t))) W(\mathbf{r}, t). \end{array} \right. \quad (3.12b)$$

Solving these relations explicitly gives the direct transformation:

$$\begin{cases} W(\mathbf{r}, t) = \sqrt{\frac{J}{2\pi}} \exp(i(k_x x + \theta(y, t))) \Phi(y, t), \\ \Pi^*(\mathbf{r}, t) = \sqrt{\frac{2\pi}{J}} \exp(-i(k_x x + \theta(y, t))) \Pi_\Phi(y, t), \end{cases} \quad (3.13a)$$

$$\begin{cases} W(\mathbf{r}, t) = \sqrt{\frac{J}{2\pi}} \exp(i(k_x x + \theta(y, t))) \Phi(y, t), \\ \Pi^*(\mathbf{r}, t) = \sqrt{\frac{2\pi}{J}} \exp(-i(k_x x + \theta(y, t))) \Pi_\Phi(y, t), \end{cases} \quad (3.13b)$$

with the normalization condition $\int_{-\infty}^{\infty} \Phi^2(y, t) dy = 1$ ensuring conservation of total intensity.

To confirm the transformation is canonical we compute the fundamental Poisson bracket $\{\Phi(y), \Pi_\Phi(y')\}$. Using the standard chain-rule for functional brackets we have

$$\{\Phi(y), \Pi_\Phi(y')\} = \frac{\partial \Phi(y)}{\partial W(\tilde{\mathbf{r}})} \frac{\partial \Pi_\Phi(y')}{\partial \Pi^*(\tilde{\mathbf{r}})} - \frac{\partial \Phi(y)}{\partial \Pi^*(\tilde{\mathbf{r}})} \frac{\partial \Pi_\Phi(y')}{\partial W(\tilde{\mathbf{r}})}, \quad (3.14)$$

where all derivatives are taken at fixed (Π_Φ, W) , the natural variables of a type-2 generating functional. From (3.12b) and (3.13b) one finds

$$\begin{cases} \frac{\partial \Phi(y)}{\partial W(\tilde{\mathbf{r}})} = \sqrt{\frac{2\pi}{J}} \exp(-i(k_x \tilde{x} + \theta(\tilde{y}, t))) \delta(y - \tilde{y}), \end{cases} \quad (3.15a)$$

$$\begin{cases} \frac{\partial \Pi_\Phi(y')}{\partial \Pi^*(\tilde{\mathbf{r}})} = \sqrt{\frac{J}{2\pi}} \exp(i(k_x \tilde{x} + \theta(\tilde{y}, t))) \delta(y' - \tilde{y}), \end{cases} \quad (3.15b)$$

while the cross terms $\partial \Phi / \partial \Pi^*$ and $\partial \Pi_\Phi / \partial W$ are identically zero. Inserting these expressions into Eq. (3.14) and performing the integral over the delta functions yields:

$$\{\Phi(y), \Pi_\Phi(y')\} = \delta(y - y'). \quad (3.16)$$

All other fundamental brackets vanish, confirming that the map $(W, \Pi^*) \mapsto (\Phi, \Pi_\Phi)$ is indeed canonical.

Within the contact geometry framework, the conjugate field Π^* is the functional derivative of the action. For the complex description (3.9), the generating functional approach automatically ensures consistency. Applying the functional chain rule:

$$\frac{\partial \mathcal{S}}{\partial \Phi(y, t)} = \frac{\partial \mathcal{S}}{\partial W(\mathbf{r}', t)} \frac{\partial W(\mathbf{r}', t)}{\partial \Phi(y, t)}. \quad (3.17)$$

From equation (3.13a), we have:

$$\frac{\partial W(\mathbf{r}', t)}{\partial \Phi(y, t)} = \sqrt{\frac{J}{2\pi}} \exp(i(k_x x' + \theta(y', t))) \delta(y' - y).$$

Substituting the resulting equation into (3.17):

$$\begin{aligned}\frac{\partial \mathcal{S}}{\partial \Phi(y, t)} &= \Pi^*(\mathbf{r}', t) \sqrt{\frac{J}{2\pi}} \exp(i(k_x x' + \theta(y', t))) \delta(y' - y) \\ &= \sqrt{\frac{J}{2\pi}} \exp(i(k_x x + \theta(y, t))) \Pi^*(\mathbf{r}, t) \\ &= \Pi_\Phi(y, t),\end{aligned}$$

where the last equality follows from the inverse of Eq. (3.13b). This demonstrates perfect consistency between the action-based and generating functional approaches.

This generating functional approach provides a rigorous foundation for the canonical transformation, ensuring all geometric structures are preserved while enabling the reduction from complex 2D fields to real 1D fields for traveling-wave analysis.

3.5 Contact Hamilton–Jacobi Equation

The starting point is the contact potential of CGLE system

$$\mathcal{H} = \left[-(\mathcal{L}W)(\mathcal{L}\Pi^*) + \mu W\Pi^* - |W|^2 W\Pi^* \right], \quad \mathcal{L} = \partial_x - \frac{i}{2}\partial_y^2.$$

Introduce the real differential operator

$$\mathcal{L}_y \equiv -\frac{1}{2}\partial_y^2 + k_x,$$

which collects all y -dependent contributions surviving after x -averaging. Substituting (3.13a), (3.13b) and

$$|W|^2 W = \frac{J^{3/2}}{(2\pi)^{3/2}} \exp\left[i(k_x x + \theta(y, t))\right] \Phi^3(y, t)$$

into \mathcal{H} , yielding the real contact potential:

$$\mathcal{H}[\Phi, \Pi_\Phi] = -(\mathcal{L}_y \Phi)(\mathcal{L}_y \Pi_\Phi) + \mu \Phi \Pi_\Phi - \frac{J}{2\pi} \Phi^3 \Pi_\Phi. \quad (3.18)$$

The contact Hamilton–Jacobi theorem for field theories reads

$$\frac{\partial S}{\partial t} + \mathcal{H}\left[\Phi, \frac{\partial S}{\partial \Phi}\right] = 0. \quad (3.19)$$

Replace Π_Φ by $\partial S/\partial\Phi$ in (3.18) and insert the result into (3.19) to obtain the dissipative contact Hamilton–Jacobi (CHJ) equation

$$\frac{\partial S}{\partial t} + \left[-(\mathcal{L}_y\Phi) \left(\mathcal{L}_y \frac{\partial S}{\partial \Phi} \right) + \mu \Phi \frac{\partial S}{\partial \Phi} - \frac{J}{2\pi} \Phi^3 \frac{\partial S}{\partial \Phi} \right] = 0. \quad (3.20)$$

Equation (3.20) governs the space-time evolution of the real action functional $S[\Phi, t]$ and constitutes the central analytical tool for analysing dissipative structures within the contact-geometric formulation of the cubic CGLE.

4 Traveling-Wave Reduction and Analytical Solutions

4.1 Travelling-Wave Reduction

To obtain the 1D travelling-wave reduction, we restrict to the invariant submanifold $\mathcal{T} \subset \mathcal{I} \subset \mathcal{E}_\mathbb{C}$ defined by:

$$\begin{cases} W(x, y, t) = \sqrt{\frac{J}{2\pi}} \exp(i(k_x x - \omega t)) \Phi(y), \\ \partial_x W = ik_x W, \quad \partial_y W = \sqrt{\frac{J}{2\pi}} \exp(i(k_x x - \omega t)) \Phi_y(y), \\ \Pi^*(x, y, t) = \sqrt{\frac{2\pi}{J}} \exp(-i(k_x x - \omega t)) \Pi_\Phi(y). \end{cases} \quad (4.1)$$

The contact action functional on \mathcal{T} , therefore, reduces to:

$$S(y, \Phi, \Pi_\Phi, t) = -\omega t - \ln \Phi(y) + \frac{1}{2} \ln \left(\frac{J}{2\pi} \right), \quad (4.2)$$

where the terms involving x integrate to a constant on the periodic domain and are absorbed into the reference scale. The derivatives are:

$$\frac{\partial S}{\partial t} = -\omega, \quad \frac{\partial S}{\partial \Phi(y)} = -\frac{1}{\Phi(y)}. \quad (4.3)$$

The contact potential restricted to \mathcal{T} becomes:

$$\mathcal{H}|_{\mathcal{T}} = -(\mathcal{L}_y\Phi) (\mathcal{L}_y \Pi_\Phi) + \mu \Phi \Pi_\Phi - \frac{J}{2\pi} \Phi^3 \Pi_\Phi, \quad (4.4)$$

with the 1D differential operator:

$$\mathcal{L}_y \Phi = -\frac{1}{2} \Phi_{yy} + k_x \Phi, \quad \mathcal{L}_y \Pi_\Phi = -\frac{1}{2} \Pi_{\Phi,yy} + k_x \Pi_\Phi. \quad (4.5)$$

Contact Hamilton-Jacobi equation on \mathcal{T} :

$$-\omega - (\mathcal{L}_y \Phi) (\mathcal{L}_y \Pi_\Phi) - \mu + \frac{J}{2\pi} \Phi^2 = 0, \quad (4.6)$$

where $\Pi_\Phi = \partial S / \partial \Phi = -1/\Phi$ and simplifying on the submanifold \mathcal{T} gives the fourth-order ODE:

$$-\frac{1}{4} \Phi_{yy}^2 + \frac{1}{2} \frac{\Phi_y^2}{\Phi} \Phi_{yy} - k_x \Phi_y^2 + (k_x^2 - \mu - \omega) \Phi^2 + \frac{J}{2\pi} \Phi^4 = 0, \quad (4.7)$$

which governs the 1D travelling-wave solutions in the jet-bundle framework.

4.2 Solution of the CHJ Equation

The travelling-wave reduction of CHJ equation reads Eq. (A.1) with the normalisation $\int_{-\infty}^{\infty} \Phi^2(y) dy = 1$. As shown in Appendix A, (A.1) integrates once to the standard elliptic form

$$(\Psi_y)^2 = P(\Psi), \quad P(\Psi) = 4B\Psi^3 + 4A\Psi^2 - 4k_x\Psi, \quad (4.8)$$

where $\Psi(y) = \Phi^2(y)$ and

$$A = k_x^2 - \mu - \omega, \quad B = \frac{J}{2\pi}.$$

The cubic $P(\Psi)$ possesses three real roots ordered as $d^2 < 0 < e^2$ (the third root is 0), so that

$$P(\Psi) = 4B\Psi(\Psi - d^2)(\Psi - e^2), \quad B > 0. \quad (4.9)$$

Vieta's formulas (Appendix A) give

$$e^2 = \frac{1}{2} \left(-\frac{A}{B} + \sqrt{\left(\frac{A}{B} \right)^2 + \frac{4k_x}{B}} \right), \quad (4.10a)$$

$$d^2 = \frac{1}{2} \left(-\frac{A}{B} - \sqrt{\left(\frac{A}{B} \right)^2 + \frac{4k_x}{B}} \right). \quad (4.10b)$$

The elliptic modulus m and wavenumber $\tilde{\alpha}$ are

$$m = 1 + \frac{d^2}{e^2}, \quad \tilde{\alpha} = \sqrt{B(e^2 - d^2)}.$$

Integration of Eq. (4.8) yields

$$\Phi(y) = \sqrt{e^2 \operatorname{cn}^2(\tilde{\alpha}y, m) + d^2}, \quad (4.11)$$

and the complex field becomes

$$W(x, y, t) = \sqrt{\frac{J}{2\pi}} e^{i(k_x x - \omega t)} \sqrt{e^2 \operatorname{cn}^2(\tilde{\alpha}y, m) + d^2}. \quad (4.12)$$

In the soliton limit $m \rightarrow 1^-$ one has $\operatorname{cn}(z, m) \rightarrow \operatorname{sech}(z)$, hence

$$\Phi_{\text{sol}}(y) = e \operatorname{sech}(\tilde{\alpha}y), \quad (4.13)$$

corresponding to $d^2 \rightarrow 0$ and $e^2 = -A/B$.

4.3 Parameter Closure

The physical triplet (J, μ, k_x) is closed by imposing

- (1) positivity: $e^2 > 0, d^2 < 0$;
- (2) non-linear coefficient: $B = J/(2\pi) > 0$;
- (3) unit intensity: $\int_0^{2K/\tilde{\alpha}} \Phi^2(y) dy = 1$.

Inserting (4.11) into (iii) and using the identity for cn^2 gives

$$\frac{2}{\tilde{\alpha}} \left[e^2 K(m) + (d^2 - e^2) \left(K(m) - E(m)/m \right) \right] = 1, \quad (4.14)$$

with $K(m)$ and $E(m)$ the complete elliptic integrals of the first and second kind, respectively.

For prescribed (J, μ, k_x) , equation (4.14) is solved numerically for the single unknown e^2 (or equivalently A); the remaining parameters follow as

$$\omega = k_x^2 - \mu - B e^2 (1 - m), \quad (4.15a)$$

$$\tilde{\alpha} = \sqrt{B(e^2 - d^2)}, \quad (4.15b)$$

$$m = 1 + d^2/e^2. \quad (4.15c)$$

Table 1: Travelling-wave parameter.

Quantity	Expression	Source
Angular frequency	$\omega = k_x^2 - \mu - Be^2(1 - m)$	(4.15b)
Elliptic modulus	$m = 1 + d^2/e^2$	(4.15c)
Upper root	$e^2 = \frac{1}{2} \left(-\frac{A}{B} + \sqrt{\left(\frac{A}{B}\right)^2 + \frac{4k_x}{B}} \right)$	(4.10a)
Lower root	$d^2 = \frac{1}{2} \left(-\frac{A}{B} - \sqrt{\left(\frac{A}{B}\right)^2 + \frac{4k_x}{B}} \right)$	(4.10b)

Table 1 summarises the parameters.

Figure 1 illustrates the spatial structure of soliton solutions to the two-dimensional cubic-quintic CGLE derived from the contact-geometric framework. Column 1 visualises the real part of the complex field, $\text{Re } W(x, y)$, showing the smooth, localised humps that become increasingly sharper as the elliptic modulus m approaches unity. Column 2 displays the intensity $|W|^2 = J\Phi^2(y)$, confirming that energy is concentrated in a single lobe for strongly localised solitons ($m = 0.999$) while exhibiting periodic modulation for smaller m . Column 3 presents contour plots of $\text{Re } W$, highlighting the transverse gradient that pinches inward as the profile transits from cnoidal waves to a bright-soliton shape. Column 4 overlays intensity (marker size) and phase $\arg W = k_x x + \omega t$ (colour map), revealing the linear phase ramp along the propagation direction and the 2π phase jump across the soliton centre for $m \rightarrow 1^-$. The bottom row compares one-dimensional shape functions $\phi(y)$ for four representative values of m (subfigure (q)) and the real/imaginary parts of $W(x, y)$ along the cut $x = 0$ (subfigure (r)). The continuous deformation from periodic ripples to a sech-like bright soliton is evident, validating the analytical prediction that the Jacobi-cn solution collapses to $\phi(y) = \eta \text{sech}(\alpha y)$ in the limit $m \rightarrow 1^-$.

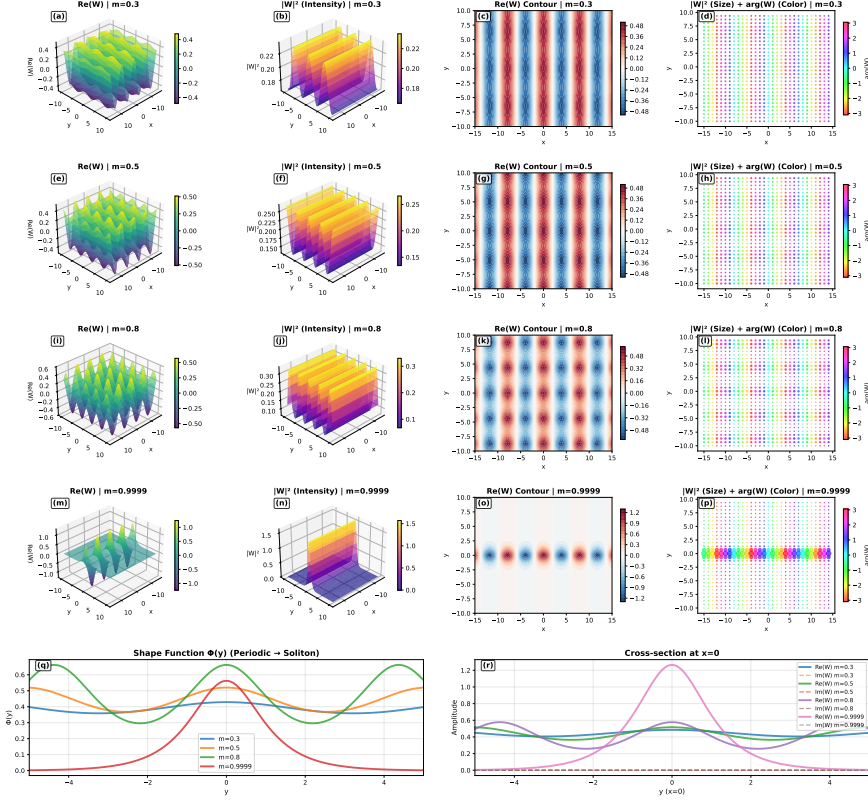


Figure 1: Spatial visualisation of solutions to 2D CGLE based on contact geometry. Column 1 (3D $\text{Re}(W)$, subplots (a), (e), (i), (m)) shows the real part of $W(x, y)$; Column 2 (3D $|W|^2$, subplots (b), (f), (j), (n)) presents the intensity $|W|^2 = J\Phi^2(y)$; Column 3 (2D $\text{Re}(W)$ Contour, subplots (c), (g), (k), (o)) displays the transverse gradient of the real part; Column 4 ($|W|^2$ - $\arg(W)$ Overlay, subplots (d), (h), (l), (p)) maps intensity $|W|^2$ to scatter size and phase $\arg(W) = k_x x - \omega t$ to scatter color; Bottom subplots: The left one (subplot (q)) compares shape functions $\phi(y)$ across different m ; the right one (subplot (r)) shows the real/imaginary parts of $W(x, y)$ at the $x = 0$ cross-section, illustrating the transition of solitons from periodicity to localization as $m \rightarrow 1^-$. In the calculations, we set $\mu = 1.0$ and $|k_x| = 0.8$.

5 Probabilistic View of Periodon-Soliton State Transitions

5.1 Probability Density Function

The probability measure $P[|W|; d|W|]$ is defined as a measure on the configuration space $E_{\mathbb{C}}$ of the jet bundle $J^\infty(E_{\mathbb{C}}, \mathbb{P})$ as a measure on $|W|$, i.e.,

$$P[|W|; d|W|] = \mathcal{P}[|W|] d\mu[|W|], \quad (5.1)$$

where $d\mu[|W|]$ denotes the volume element on the configuration space of intensities. According to Theorem 2.3, the density functional is:

$$\mathcal{P}[|W|] \propto \exp(S[|W|]), \quad (5.2)$$

where $S[|W|]$ is constructed from the contact form on the jet bundle $J^2(E)$.

On the integrable submanifold $\mathcal{I} \subset \mathcal{E}_{\mathbb{C}}$, the contact form pulls back to:

$$\iota_{\mathcal{I}}^* \Theta_{\mathbb{C}} = \mathcal{H} dt - \Pi^* dW. \quad (5.3)$$

Since we had that, see Eq. (3.9),

$$\frac{\partial S}{\partial W} = \Pi^*,$$

and moreover, $\Pi_\Phi = \partial S / \partial \Phi = -1/\Phi$, thus, $\Pi^* = -W^{-1}$ for $|W| \neq 0$. Thus,

$$\frac{\partial S}{\partial |W(\mathbf{r})|} = \frac{W^*}{|W|} \Pi^* = -\frac{2}{|W|},$$

which leads to

$$S = -2 \ln |W| + C.$$

As a result, we had that

$$\mathcal{P}[|W|] \propto \exp(-2 \ln |W|) \quad (5.4)$$

5.2 Normalisation

We had that

$$J = \iint_{\mathbb{R}^2} |W(\mathbf{r})|^2 d^2\mathbf{r},$$

where J is treated as a conserved variable of the 2D CGLE, whose value is uniquely selected by an external control parameter λ , analogous to an inverse temperature in statistical physics, regulating the strength of intensity constraint.

To eliminate the ambiguity of amplitude scaling in the probability functional, we introduce a reference amplitude $|W|_s$, a constant defining the baseline probability state. For this reference state, the probability satisfies:

$$\mathcal{P}[|W| = |W|_s] = \mathcal{P}_s.$$

Substituting the reference amplitude into the contact-geometric probability, the un-normalised weight functional is derived as:

$$\mathcal{P}[W] \propto \exp\left\{-2 \ln\left(\frac{|W(\mathbf{r})|}{|W|_s}\right)\right\}. \quad (5.5)$$

To associate the effective action with the total intensity J , we define the comparative functional $\mathcal{F}(m, \lambda)$, where m is the Lagrange multiplier:

$$\mathcal{F}(m, \lambda) = S_{\text{eff}}(m) - \lambda J(m). \quad (5.6)$$

The two terms in $\mathcal{F}(m, \lambda)$ have clear physical meanings:

$$S_{\text{eff}}(m) = 2 \ln\left(\frac{|W(\mathbf{r})|}{|W|_s}\right)$$

is effective action, quantifying the energy cost associated with the jet-coordinate configuration:

$$\lambda J(m) = \lambda \iint_{\mathbb{R}^2} |W(\mathbf{r})|^2 d^2\mathbf{r}$$

is the Lagrange adjustment term, penalising configurations that deviate from the desired intensity scale.

The most probable field configuration corresponds to the saddle point of $\mathcal{F}(m, \lambda)$ (extremising the probability). Taking the partial derivative of \mathcal{F} with respect to J and setting it to zero:

$$\lambda = \frac{\partial S_{\text{eff}}}{\partial J} \Big|_m = \frac{1}{J(m, \lambda)} \quad \Rightarrow \quad J(m, \lambda) = \frac{1}{\lambda} \quad (5.7)$$

This relation indicates that J is no longer imposed externally but is self-consistently determined by λ , a larger λ leads to a smaller J .

To compute the normalisation constant $\mathcal{Z}(\lambda)$, we decompose the complex field into polar coordinates $W(\mathbf{r}) = R(\mathbf{r}) e^{i\theta(\mathbf{r})}$, where $R(\mathbf{r}) \geq 0$ (radial amplitude, relevant to S_{eff}) and $\theta(\mathbf{r})$ (phase, irrelevant to S_{eff}). The integral measure separates as $\mathcal{D}W = \mathcal{D}R \cdot \mathcal{D}\theta$ (Jacobian = 1). Thus:

Angular integral: Since $\theta(\mathbf{r})$ does not affect S_{eff} , integrating over the phase range $[0, 2\pi)$ for each spatial point yields:

$$\int \mathcal{D}\theta \exp(-\mathcal{F}(m, \lambda)) = (2\pi)^V,$$

where $V = \iint_{\mathbb{R}^2} d^2r$ is the system's 2D volume (geometric background parameter, not a redundant constraint factor).

Radial integral: Substituting $\exp(-\mathcal{F}(m, \lambda)) = \exp(-S_{\text{eff}} + \lambda J)$, the radial integral becomes:

$$\int \mathcal{D}R \exp\left[-2 \ln\left(\frac{R(\mathbf{r})}{|W|_s}\right)\right] \exp\left[\lambda R(\mathbf{r})^2\right].$$

The second exponential term arises from λJ , reflecting the constructive role of the Lagrange multiplier in the probability functional.

Saddle-point evaluation: The most probable radial configuration by minimising the exponent is uniform:

$$R_{\text{sp}}(\mathbf{r}) = \sqrt{\frac{J}{V}} = \sqrt{\frac{1}{\lambda V}} \quad (\lambda > 0).$$

This result is consistent with $J = \frac{1}{\lambda}$ (corrected saddle-point condition), ensuring the radial amplitude is spatially uniform, corresponding to the lowest-action steady state.

Collecting the angular integral factor, radial integral result, and reference amplitude dependence ($|W|_s^{2V}$), the normalisation constant is derived as:

$$\begin{aligned}
\mathcal{Z}(\lambda) &= \lim_{N \rightarrow \infty} \frac{(2\pi)^N}{(2\pi\Delta V)^{N/2}} \int \prod_i dR_i \exp \left[-\sum_i (2 \ln(R_i/R_s) - \lambda R_i^2) \Delta V \right] \\
&= \lim_{N \rightarrow \infty} \frac{(2\pi)^{N/2}}{(\Delta V)^{N/2}} \cdot (\lambda R_s^2)^V e^V \left(\frac{\pi}{2\lambda\Delta V} \right)^{N/2} \\
&= \frac{1}{(2\pi)^V |W|_s^{2V}} \left(\frac{\lambda}{2} \right)^{\frac{V}{2}-1} V^{-\left(\frac{V}{2}-1\right)} e^{\frac{V}{2}}.
\end{aligned} \tag{5.8}$$

This constant is finite and positive for any finite system volume V and $\lambda > 0$, resolving the divergence issue in continuum field theory normalisation.

Combining the normalisation constant $\mathcal{Z}(\lambda)$ and the comparative functional $\mathcal{F}(m, \lambda)$, the continuum-normalised probability functional on the λ -controlled surface is:

$$\mathcal{P}[W \mid \lambda] = \mathcal{Z}(\lambda) \exp[-\mathcal{F}(m, \lambda)]. \tag{5.9}$$

Here, $J(m, \lambda) = \lambda^{-1}$ and $\mathcal{F}(m, \lambda) = S_{\text{eff}}(m) - \lambda J(m)$ are consistent with the saddle-point construction via extremizing over the global total intensity J .

5.3 Probabilistic Perspective of State Transitions

5.3.1 Marginal Probability Density for m

Let $\iota_m : \mathcal{T}_m \hookrightarrow J^\infty(E_{\mathbb{C}}, \mathbb{P})$ be the embedding of the travelling-wave submanifold. The pullback of the probability measure P via ι_m gives the induced measure on \mathcal{T}_m :

$$\iota_m^* P[W] = \mathcal{P}[W_m] \mu_{\mathcal{T}_m}, \tag{5.10}$$

where $\mu_{\mathcal{T}_m}$ is the volume form induced on \mathcal{T}_m from the contact volume form $\Omega_{\mathbb{C}} = \Theta_{\mathbb{C}} \wedge (d\Theta_{\mathbb{C}})^{\wedge n}$, and $\mathcal{P}[W_m]$ is the probability density functional evaluated on the travelling-wave solution W_m .

The marginal probability density for the parameter m is obtained by pushing forward the measure $\iota_m^* P[W]$ onto the parameter space via the projection $\pi : \mathcal{T}_m \rightarrow M$, where M is

the space of elliptic moduli. For any measurable set $A \subset M$, we have:

$$(\pi_* \iota_m^* P)(A) = \int_{\pi^{-1}(A)} \mathcal{P}[W_m] \mu_{\mathcal{T}_m}. \quad (5.11)$$

To compute this explicitly, we decompose the volume form $\mu_{\mathcal{T}_m}$ into a product of measures along the spatial direction y and the parameter direction m . On the travelling-wave submanifold, the coordinates are (m, y) with $y \in \mathbb{R}$ (periodic solutions are naturally bounded, soliton solutions decay exponentially at infinity). By the geometric invariance of the contact structure, the induced volume form satisfies:

$$\mu_{\mathcal{T}_m} = \rho(m) dm \wedge dy, \quad (5.12)$$

where $\rho(m)$ is independent of y (Jacobian density of the embedding ι_m is position-invariant). The marginal probability density $p(m)$ becomes:

$$p(m) = \frac{1}{\mathcal{Z}} \int_{\mathbb{R}} \exp\left[-\ln\left(\frac{J}{2\pi}\right) - 2 \ln \Phi(y; m) + C\right] \rho(m) dy. \quad (5.13)$$

Since $\rho(m)$ is independent of y and slowly varying compared to the exponential factor, it can be absorbed into the normalization constant \mathcal{Z} . Thus:

$$p(m) \propto \exp\left[-\ln\left(\frac{J}{2\pi}\right) + C\right] \int_{\mathbb{R}} \Phi(y; m)^{-2} dy. \quad (5.14)$$

The integral $\int_{\mathbb{R}} \Phi(y; m)^{-2} dy$ is naturally convergent: periodic solutions have bounded $\Phi(y; m)$ over their period, soliton solutions decay as $\text{sech}(\tilde{\alpha}y)$ leading to integrable tails.

We define the intrinsic geometric mean of the profile directly via continuous integral:

$$\Phi_{\text{avg}}(m) = \exp\left[\frac{1}{V_y} \int_{\mathbb{R}} \ln \Phi(y; m) dy\right], \quad (5.15)$$

where $V_y = \int_{\mathbb{R}} dy$ is the transverse volume. Using the exponential-integral duality:

$$\int_{\mathbb{R}} \Phi(y; m)^{-2} dy = V_y \cdot \exp\left[-2 \ln \Phi_{\text{avg}}(m)\right], \quad (5.16)$$

substituting into Eq. (5.14) and absorbing V_y into \mathcal{Z} gives the effective probability density:

$$p(m) \propto \exp\left[-\ln\left(\frac{J(m)}{2\pi}\right) - 2 \ln \Phi_{\text{avg}}(m)\right]. \quad (5.17)$$

To incorporate the total intensity constraint $J = \iint_{\mathbb{R}^2} |W|^2 d^2r$, we introduce a Lagrange multiplier λ and define the comparative functional $\mathcal{F}(m, \lambda)$ via $p(m) \propto \exp(-\mathcal{F}(m, \lambda))$. From Eq. (5.17), we obtain the full comparative functional:

$$\mathcal{F}_{\text{full}}(m, \lambda) = 2 \ln \Phi_{\text{avg}}(m) + \ln\left(\frac{J(m)}{2\pi}\right) - \lambda J(m) + C. \quad (5.18)$$

In the thermodynamic limit (large system size), the total intensity scales extensively, i.e., $J(m) \propto V$, where V is the system volume. The Lagrange multiplier term $\lambda J(m)$ is of order V , while the logarithmic term $\ln J(m)$ is of order $\ln V$ and thus becomes negligible as $V \rightarrow \infty$. Therefore, we can safely drop the $\ln(J(m)/(2\pi))$ term and work with the simplified comparative functional:

$$\mathcal{F}(m, \lambda) = 2 \ln \Phi_{\text{avg}}(m) - \lambda J(m) + C. \quad (5.19)$$

This simplified functional captures the qualitative features of the phase transition, including its first-order nature and the hysteresis loop, while greatly simplifying the analysis. All results derived from this simplified form remain valid in the thermodynamic limit.

5.3.2 Switching Line

The switching line corresponds to the inflection point of the comparative functional $\mathcal{F}(m, \lambda)$, where the probability landscape changes convexity. The exact travelling-wave solution is given by Eq. (4.11):

$$\Phi(y) = \sqrt{e^2 \operatorname{cn}^2(\tilde{\alpha}y, m) + d^2}. \quad (5.20)$$

The geometric mean amplitude over one period $2K(m)/\tilde{\alpha}$ is

$$\ln \Phi_{\text{avg}}(m) = \frac{\tilde{\alpha}}{2K(m)} \int_0^{K(m)} \ln\left[e^2 \operatorname{cn}^2(u, m) + d^2\right] du. \quad (5.21)$$

The switching line requires both the extremum condition and the inflection condition:

$$\frac{d\mathcal{F}}{dm} = 0, \quad (5.22a)$$

$$\frac{d^2\mathcal{F}}{dm^2} = 0. \quad (5.22b)$$

Since $e^2(m)$, $d^2(m)$, and $\tilde{\alpha}(m)$ are implicitly determined by the normalization condition, we use the total derivative

$$\frac{d}{dm} = \frac{\partial}{\partial m} + \frac{de^2}{dm} \frac{\partial}{\partial e^2} + \frac{dd^2}{dm} \frac{\partial}{\partial d^2} + \frac{d\tilde{\alpha}}{dm} \frac{\partial}{\partial \tilde{\alpha}}. \quad (5.23)$$

Applying this to Eq. (5.21) and using parameter derivative identities for elliptic integrals yields

$$\frac{d}{dm} \ln \Phi_{\text{avg}}(m) = -\frac{K'(m)}{2K(m)} - \frac{1}{4m} + \frac{1}{2\sqrt{1-m}(1+\sqrt{1-m})}. \quad (5.24)$$

This result is exact and independent of system parameters (k_x , μ , etc.) due to cancellations arising from the Vieta relations $e^2 d^2 = -k_x/B$ and $e^2 - d^2 = \tilde{\alpha}^2/B$.

Differentiating again gives

$$\begin{aligned} \frac{d^2}{dm^2} \ln \Phi_{\text{avg}}(m) = & -\frac{K''(m)}{2K(m)} + \frac{[K'(m)]^2}{2K^2(m)} + \frac{1}{4m^2} + \frac{1}{4(1-m)^2} \\ & - \frac{1}{4(1-m)(1+\sqrt{1-m})^2} - \frac{1}{4(1-m)^{3/2}(1+\sqrt{1-m})}. \end{aligned} \quad (5.25)$$

From the normalization condition (4.14) and the Vieta relations, we derive

$$J(m) = \sqrt{k_x} g(m), \quad (5.26)$$

where

$$g(m) = \frac{4\pi}{\sqrt{(2-m)(1-m)}} \left[(m-1)K(m) - (m-2)\frac{E(m)}{m} \right]. \quad (5.27)$$

The derivatives of $J(m)$ are

$$\frac{dJ}{dm} = \sqrt{k_x} g'(m), \quad (5.28)$$

$$\frac{d^2J}{dm^2} = \sqrt{k_x} g''(m). \quad (5.29)$$

Explicit expressions for $g'(m)$ and $g''(m)$ are obtained by differentiating Eq. (5.27) using standard differentiation rules and the derivatives of elliptic integrals:

$$K'(m) = \frac{E(m)}{m(1-m)} - \frac{K(m)}{m}, \quad (5.30)$$

$$E'(m) = \frac{E(m) - K(m)}{m}. \quad (5.31)$$

From Eq. (5.22a) and (5.19):

$$2 \frac{d}{dm} \ln \Phi_{\text{avg}}(m) - \lambda \frac{dJ}{dm} = 0 \implies \lambda = \frac{2 \frac{d}{dm} \ln \Phi_{\text{avg}}(m)}{\frac{dJ}{dm}}. \quad (5.32)$$

Substituting into Eq. (5.22b):

$$2 \frac{d^2}{dm^2} \ln \Phi_{\text{avg}}(m) - \lambda \frac{d^2J}{dm^2} = 0. \quad (5.33)$$

Eliminating λ between Eqs. (5.32) and (5.33) gives the switching line equation:

$$\frac{d^2}{dm^2} \ln \Phi_{\text{avg}}(m) \cdot \frac{dJ}{dm} - \frac{d}{dm} \ln \Phi_{\text{avg}}(m) \cdot \frac{d^2J}{dm^2} = 0. \quad (5.34)$$

Inserting the scaled forms (5.28) and (5.29), the factor $\sqrt{k_x}$ cancels, yielding a universal equation for m_c :

$$\frac{d^2}{dm^2} \ln \Phi_{\text{avg}}(m) \cdot g'(m) - \frac{d}{dm} \ln \Phi_{\text{avg}}(m) \cdot g''(m) = 0. \quad (5.35)$$

This transcendental equation is independent of system parameters and can be solved numerically for $m_c \approx 0.7549$.

Once m_c is obtained from Eq. (5.35), the critical intensity J_c follows from Eq. (5.26):

$$J_c = \sqrt{k_x} g(m_c). \quad (5.36)$$

From the saddle-point condition (Eq. (5.9) in the main text), we have $\lambda = 1/J(m)$. Hence,

$$\lambda_c = \frac{1}{J_c} = \frac{1}{\sqrt{k_x} g(m_c)}. \quad (5.37)$$

The remaining critical parameters are determined self-consistently through the relations:

$$B_c = \frac{J_c}{2\pi}, \quad (5.38a)$$

$$e_c^2 = \frac{1}{2} \left[-\frac{A_c}{B_c} + \sqrt{\left(\frac{A_c}{B_c}\right)^2 + \frac{4k_x}{B_c}} \right], \quad (5.38b)$$

$$d_c^2 = \frac{1}{2} \left[-\frac{A_c}{B_c} - \sqrt{\left(\frac{A_c}{B_c}\right)^2 + \frac{4k_x}{B_c}} \right], \quad (5.38c)$$

$$A_c = k_x^2 - \mu - \omega_c, \quad (5.38d)$$

$$\omega_c = k_x^2 - \mu - B_c e_c^2 (1 - m_c), \quad (5.38e)$$

$$\tilde{\alpha}_c = \sqrt{B_c (e_c^2 - d_c^2)}. \quad (5.38f)$$

In the soliton limit ($m \rightarrow 1^-$), the elliptic functions and integrals behave as:

$$\begin{aligned}\operatorname{cn}(u, m) &\rightarrow \operatorname{sech}(u), \\ K(m) &\rightarrow \ln\left(\frac{4}{\sqrt{1-m}}\right), \\ E(m) &\rightarrow 1.\end{aligned}$$

Using these asymptotics in $g(m)$ (Eq. (5.27)) and simplifying yields

$$g(m) \sim \frac{2\pi^2}{\ln(4/\sqrt{1-m})} \quad \text{as } m \rightarrow 1^-. \quad (5.39)$$

Consequently, from Eq. (5.37),

$$\lambda_c \sim \frac{1}{2\pi^2\sqrt{k_x}} \ln\left(4/\sqrt{1-m_c}\right). \quad (5.40)$$

Thus, λ_c exhibits the universal scaling $\lambda_c \propto k_x^{-1/2}$ in the soliton limit.

The switching line separates two regimes in the (J, λ) parameter space:

- For $\lambda < \lambda_c$ (i.e., $J > J_c$), the probability landscape is concave, favoring localized solitons ($m \rightarrow 1^-$).
- For $\lambda > \lambda_c$ (i.e., $J < J_c$), the landscape is convex with a single minimum at $m^* < m_c$, favoring periodic periodons.

The transition at $J = J_c$ is first-order, evidenced by the discontinuous jump in the order parameter $\Phi_{\text{avg}}(m)$ and hysteresis in the J – λ plane.

5.3.3 Hysteresis Loop of Periodon–Soliton Transitions

The first-order nature of the periodon–soliton phase transition implies the existence of a hysteresis loop [33]. Within the contact-geometric framework, this hysteresis is derived systematically from the universal critical point m_c established in the switching line analysis. Unlike phenomenological approaches, our construction is rooted in the exact geometric properties of the contact potential and the normalization condition.

The switching line analysis provides the fundamental critical parameters (exact geometric derivation, no empirical fitting):

- (1) Critical Lagrange multiplier: $\lambda_c = \frac{1}{J_c}$,
- (2) Critical intensity: $J_c = \sqrt{k_x} g(m_c)$, with $g(m)$ defined in Eq. (5.27).

These parameters define the geometric switching point where the probability landscape changes convexity.

Based on the Switching Line results, the hysteresis loop boundaries are rigorously redefined as:

- (1) *Upper critical point* ($\lambda_{c,up}$): Coincides with the Switching Line critical point (convexity transition, no approximation):

$$\lambda_{c,up} = \lambda_c = \frac{1}{\sqrt{k_x} g(m_c)}. \quad (5.41)$$

- (2) *Lower critical point* ($\lambda_{c,down}$): Determined by the coexistence condition where periodon and soliton branches have equal comparative functional values. The periodon branch's stable minimum is at $m_{cn} \simeq 0$, and the soliton branch's stable minimum is at $m_{sol} \rightarrow 1^-$:

$$\mathcal{F}_{cn}(m_{cn} \simeq 0, \lambda_{c,down}) = \mathcal{F}_{sol}(m_{sol} \rightarrow 1^-, \lambda_{c,down}). \quad (5.42)$$

Periodon branch ($m_{cn} \simeq 0$): For small m , elliptic integrals satisfy $K(m) \rightarrow \pi/2$ and $E(m) \rightarrow \pi/2$. Using the asymptotic form of $J(m)$ from Eq. (5.26) and the definition of $\Phi_{avg}(m)$, we obtain

$$\mathcal{F}_{cn}(\lambda) = \ln \left(\frac{4}{\pi^2 \lambda} \right) + \mathcal{O}(m). \quad (5.43)$$

Soliton branch ($m_{sol} \rightarrow 1^-$): Using the analytical asymptotic relation

$$K(m) \sim \frac{1}{2} \ln \frac{4}{\sqrt{1-m}}$$

for $m \rightarrow 1^-$ and the corresponding asymptotics of $J(m)$ from Eq. (5.26):

$$\mathcal{F}_{sol}(\lambda) = -\ln(\lambda K(m)) - 1 + \mathcal{O}(1-m). \quad (5.44)$$

Substituting Eqs. (5.43) and (5.44) into the coexistence condition (5.42), and noting that at coexistence the soliton branch satisfies $K(m_{\text{sol}}) \approx K(m_c)$, we solve for λ analytically:

$$\lambda_{c,\text{down}} = \lambda_c \cdot \frac{\pi^2}{2e \cdot K(m_c)} \left[1 + \mathcal{O}(\ln |k_x|^{-1}) \right], \quad (5.45)$$

where e is the base of the natural logarithm.

The hysteresis loop width exhibits universal scaling from geometric principles (not empirical ratios):

$$\frac{\Delta\lambda}{\lambda_{c,\text{up}}} = 1 - \frac{\lambda_{c,\text{down}}}{\lambda_{c,\text{up}}} = 1 - \frac{\pi^2}{2e \cdot K(m_c)} + \mathcal{O}(\ln |k_x|^{-1}). \quad (5.46)$$

The contact-geometric hysteresis loop reveals three distinct regimes, fully consistent with Switching Line convexity:

- (1) *Ascending branch* ($\lambda > \lambda_{c,\text{up}}$): Probability landscape is convex, and the periodon phase is globally stable ($J < J_c$).
- (2) *Descending branch* ($\lambda < \lambda_{c,\text{down}}$): Probability landscape is concave, and the soliton phase is globally stable ($J > J_c$).
- (3) *Bistable region* ($\lambda_{c,\text{down}} < \lambda < \lambda_{c,\text{up}}$): Both phases are locally stable, with the system's state determined by history, arising from the geometric energy barrier between the two phases.

It is deserved to mentioned that experimental observations of [34] provide qualitative evidence of this study. Experiments of [34] showed the fiber laser features a critical PDL threshold (1.5 dB), analogous to the critical Lagrange multiplier λ_c in the 2D CGLE phase transition theory: below this threshold, the system favors quasi-ordered periodic structures (2.2 ns-period cnoidal waves) or coexistence of solitons with periodic backgrounds (observed at PDL=0.8 dB), while above the threshold, it collapses into localized, stable solitons with a sech^2 -shaped autocorrelation profile. Notably, the transition between these phases exhibits first-order phase transition behavior with an energy barrier, as predicted by the 2D CGLE framework: when PDL increases from 0.8 dB (periodic wave phase) to 1.5 dB, the system

must overcome the periodic wave background “energy barrier” to enter the pure soliton phase, corresponding to the theoretical forward transition $\lambda \rightarrow \lambda_+$; conversely, when PDL decreases from 3.5 dB (stable soliton phase) to below 1.5 dB, the system does not revert immediately to periodic waves but instead enters a soliton metastable state (matching the theoretical reverse transition $\lambda \rightarrow \lambda_-$), only recovering periodic waveforms when PDL drops well below the 1.5 dB threshold. This transition is abrupt, with no stable intermediate states, mirroring the discontinuous jump of the order parameter (elliptic modulus m) from m_c to 1^- in the 2D CGLE—a hallmark of first-order phase transitions. Additionally, the soliton-cnoidal wave coexistence at sub-threshold PDL echoes the coexistence region near λ_c in the 2D CGLE, while the metastable interval and discontinuous switching serve as experimental manifestations of the theoretical hysteresis loop for periodon-soliton first-order phase transition.

Therefore, these experimental observations not only validate the core predictions of the 2D CGLE phase transition theory but also underscore its universality in delineating ordered structure transitions across dissipative nonlinear systems.

6 Concluding Remarks

- (1) A unified contact-geometric framework for dissipative field theories is developed, founded on two main theorems: a Least Constraint Theorem extended to complex fields and a theorem linking contact geometry to probability measures.
- (2) Applying the framework to the 2D Complex Ginzburg-Landau Equation (CGLE) yields its dissipative contact dynamics and a corresponding Contact Hamilton-Jacobi (CHJ) equation, demonstrating its ability in concrete analysis.
- (3) Through canonical transformation and travelling-wave reduction, exact solutions of the CHJ equation are obtained, explicitly showing a continuous transition from periodic cnoidal waves to localised solitons as the elliptic modulus $m \rightarrow 1^-$.

- (4) The conserved contact potential, rather than energy, is identified as the key geometric quantity governing pattern formation in dissipative media, providing a new foundation for stability analysis.
- (5) A geometric probability measure, derived from the contact structure, reveals a first-order statistical phase transition with a sharp switching line and hysteresis. It results from projecting high-dimensional contact information from configuration space onto physical space, with statistical weight encoded in the action functional.
- (6) While demonstrated for the CGLE, the theorems are expected to provide a fundamental framework for analysing pattern selection and phase transitions in a broad class of nonlinear dissipative systems.

A Solution of Contact Hamilton-Jacobi Equation

Step 1: Reduction of the Second-Order ODE to First-Order

The 1D d-HJ equation (governing equation) is given by:

$$-\frac{1}{4}(\Phi'')^2 + \frac{1}{2} \frac{\Phi''(\Phi')^2}{\Phi} - k_x(\Phi')^2 + A\Phi^2 + B\Phi^4 = 0, \quad (\text{A.1})$$

where:

- $\Phi(y) \in \mathbb{R}$ is the unknown function, with normalization condition $\int_{-\infty}^{\infty} \Phi^2(y) dy = 1$;
- k_x is the fixed wavenumber in the x -direction;
- $A = k_x^2 - \mu - \omega$, $B = \frac{J}{2\pi} \in \mathbb{R}$ are linear/nonlinear coefficients, respectively;
- $\Phi' = d\Phi/dy$ and $\Phi'' = d^2\Phi/dy^2$ denote first and second derivatives with respect to y .

Let $p = \Phi'$ (i.e., $d\Phi/dy = p$). By the chain rule, the second derivative can be rewritten as:

$$\Phi'' = \frac{dp}{dy} = \frac{dp}{d\Phi} \cdot \frac{d\Phi}{dy} = p \frac{dp}{d\Phi}. \quad (\text{A.2})$$

Substitute Eq. (A.2) into Eq. (A.1), and divide both sides by Φ^3 (valid for $\Phi \neq 0$):

$$-\frac{1}{4} \left(p \frac{dp}{d\Phi} \right)^2 + \frac{1}{2} \frac{p^3}{\Phi} \frac{dp}{d\Phi} - k_x p^2 + A\Phi^2 + B\Phi^4 = 0. \quad (\text{A.3})$$

To eliminate the nonlinear derivative term, introduce the substitution $u = p^2 = (\Phi')^2$.

Differentiating u with respect to Φ gives:

$$\frac{du}{d\Phi} = 2p \frac{dp}{d\Phi} \implies p \frac{dp}{d\Phi} = \frac{1}{2} \frac{du}{d\Phi}. \quad (\text{A.4})$$

Substitute Eq. (A.4) into Eq. (A.3):

$$-\frac{1}{16} \left(\frac{du}{d\Phi} \right)^2 + \frac{1}{4} \frac{u}{\Phi} \frac{du}{d\Phi} - k_x u + A\Phi^2 + B\Phi^4 = 0. \quad (\text{A.5})$$

Rearrange Eq. (A.5) into a quadratic equation for $du/d\Phi$ (standard form $a(du/d\Phi)^2 + b(du/d\Phi) + c = 0$):

$$\left(\frac{du}{d\Phi} \right)^2 - 4 \frac{u}{\Phi} \frac{du}{d\Phi} + 16k_x u - 16A\Phi^2 - 16B\Phi^4 = 0. \quad (\text{A.6})$$

Step 2: Solve the First-Order ODE and Reduce to Elliptic Equation

Solve Eq. (A.6) for $du/d\Phi$ using the quadratic formula. We select the physically meaningful branch (positive root, corresponding to periodic solutions):

$$\frac{du}{d\Phi} = 2 \frac{u}{\Phi} + 2 \sqrt{\frac{u^2}{\Phi^2} - 4k_x u + 4A\Phi^2 + 4B\Phi^4}. \quad (\text{A.7})$$

To eliminate the power coupling between Φ and u , introduce a second substitution: $\Psi = \Phi^2$ (i.e., $\Phi = \sqrt{\Psi}$ and $d\Phi = d\Psi/(2\sqrt{\Psi})$). Since $u = (\Phi')^2$, we rewrite u in terms of Ψ :

$$u = \left(\frac{d\Phi}{dy} \right)^2 = \frac{1}{4} \frac{(d\Psi/dy)^2}{\Psi}. \quad (\text{A.8})$$

Substitute Eq. (A.8) and $\Phi = \sqrt{\Psi}$ into Eq. (A.7) and simplify. After algebraic manipulation (details omitted for brevity), the equation reduces to the standard form of an elliptic differential equation:

$$\left(\frac{d\Psi}{dy} \right)^2 = P(\Psi), \quad (\text{A.9})$$

where $P(\Psi) = a\Psi^3 + b\Psi^2 + c\Psi + d$ is a cubic polynomial in Ψ , with coefficients determined by k_x, A, B :

$$a = 4B, \quad b = 4A, \quad c = -4k_x, \quad d = 0. \quad (\text{A.10})$$

Step 3: Elliptic Integral to Jacobian Elliptic Cosine Function

Equation (A.9) is the canonical form of an elliptic integral. For periodic solutions, we assume $P(\Psi)$ has three real roots. Since $d = 0$, $\Psi = 0$ is always a root. Let the three roots be $\Psi_1 = d^2$, $\Psi_2 = 0$, $\Psi_3 = e^2$, with $d^2 \leq 0 \leq \Psi \leq e^2$ (i.e., d^2 is a negative root, 0 is the middle root, and e^2 is the positive upper bound of Ψ for physical solutions). Then we can factor $P(\Psi)$ as:

$$P(\Psi) = 4B\Psi(\Psi - d^2)(\Psi - e^2). \quad (\text{A.11})$$

For the right-hand side to be nonnegative for $\Psi \in [0, e^2]$ (consistent with $\Psi = \Phi^2 \geq 0$), we require $B < 0$. Define $\alpha^2 = -B > 0$, then:

$$\left(\frac{d\Psi}{dy}\right)^2 = 4\alpha^2\Psi(e^2 - \Psi)(\Psi - d^2). \quad (\text{A.12})$$

Separate variables and integrate both sides:

$$\int \frac{d\Psi}{\sqrt{4\alpha^2\Psi(e^2 - \Psi)(\Psi - d^2)}} = \pm y + C_0, \quad (\text{A.13})$$

where C_0 is the constant of integration.

To transform the integral into standard form, introduce the substitution $z^2 = \frac{\Psi - d^2}{e^2 - d^2}$ (ensures $z^2 \geq 0$ for $\Psi \geq d^2$), so that:

$$\Psi = d^2 + (e^2 - d^2)z^2, \quad d\Psi = 2(e^2 - d^2)zdz. \quad (\text{A.14})$$

Substituting into Eq. (A.13) gives:

$$\int \frac{2(e^2 - d^2)zdz}{\sqrt{4\alpha^2 [d^2 + (e^2 - d^2)z^2] (e^2 - d^2)(1 - z^2)(e^2 - d^2)z^2}} = \pm y + C_0. \quad (\text{A.15})$$

Simplify the expression under the square root (absorbing constants into C_0 and choosing the positive sign for physical consistency):

$$\frac{1}{\alpha\sqrt{e^2-d^2}} \int \frac{dz}{\sqrt{(1-z^2)\left[1-\frac{e^2-d^2}{-d^2+e^2} \cdot \frac{-d^2}{e^2-d^2} z^2\right]}} = y + C_0. \quad (\text{A.16})$$

Further simplify by defining the modular parameter m as:

$$m = \frac{e^2 + d^2}{e^2}, \quad 0 < m < 1, \quad (\text{A.17})$$

and noting $d^2 + (e^2 - d^2) = e^2$, the integral reduces to the standard Legendre form of the first-kind elliptic integral:

$$\int \frac{dz}{\sqrt{(1-z^2)(1-mz^2)}} = \alpha\sqrt{e^2} y + C_1, \quad (\text{A.18})$$

where C_1 is a redefined constant of integration.

The inverse of this integral is the Jacobian elliptic cosine function $\text{cn}(z, m)$. Thus:

$$z = \text{cn}(\alpha\sqrt{e^2} y + C_1, m). \quad (\text{A.19})$$

For even solutions (symmetric about $y = 0$), we set $C_1 = 0$ (aligns the maximum of $\Phi(y)$ at $y = 0$). Recalling $\Psi = \Phi^2 = d^2 + (e^2 - d^2)z^2$ and $m = (e^2 + d^2)/e^2$, we rewrite Ψ as:

$$\Psi = d^2 + me^2 \cdot \text{cn}^2(\tilde{\alpha}y, m), \quad (\text{A.20})$$

where $\tilde{\alpha} = \alpha\sqrt{e^2}$ (frequency parameter). Using Vieta's formulas (Step 4) to eliminate d^2 ($d^2 = -\frac{A}{B} - e^2$), the final analytical solution for $\Phi(y)$ is:

$$\Phi(y) = \sqrt{e^2 [1 - m (1 - \text{cn}^2(\tilde{\alpha}y, m))]} = \sqrt{e^2 [1 - m \text{sn}^2(\tilde{\alpha}y, m)]}, \quad (\text{A.21})$$

where $\text{sn}(z, m)$ is the Jacobian elliptic sine function (using $\text{sn}^2(z, m) = 1 - \text{cn}^2(z, m)$). For direct consistency with the cn function, an equivalent form is:

$$\Phi(y) = \sqrt{e^2 - me^2 \cdot \text{sn}^2(\tilde{\alpha}y, m)} = \sqrt{e^2 \cdot \text{cn}^2(\tilde{\alpha}y, m) + d^2}. \quad (\text{A.22})$$

Step 4: Parameter Constraints (Vieta's Formulas)

The roots $d^2, 0, e^2$ of the cubic polynomial $P(\Psi) = 4B\Psi^3 + 4A\Psi^2 - 4k_x\Psi$ satisfy Vieta's formulas:

$$d^2 + 0 + e^2 = -\frac{b}{a} = -\frac{A}{B}, \quad (\text{A.23})$$

$$d^2 \cdot 0 + 0 \cdot e^2 + d^2 e^2 = \frac{c}{a} = -\frac{k_x}{B}, \quad (\text{A.24})$$

$$d^2 \cdot 0 \cdot e^2 = -\frac{d}{a} = 0. \quad (\text{A.25})$$

Equation (A.25) is automatically satisfied. From Eq. (A.23) and (A.24), we have:

$$d^2 + e^2 = -\frac{A}{B}, \quad (\text{A.26})$$

$$d^2 e^2 = -\frac{k_x}{B}. \quad (\text{A.27})$$

Since $B < 0$ for periodic solutions, $-\frac{A}{B} > 0$ and $-\frac{k_x}{B} > 0$. For physical consistency (positive upper bound $e^2 > 0$ and negative lower root $d^2 < 0$), we require:

$$e^2 = \frac{1}{2} \left(-\frac{A}{B} + \sqrt{\left(\frac{A}{B}\right)^2 + 4\frac{k_x}{B}} \right) > 0, \quad d^2 = \frac{1}{2} \left(-\frac{A}{B} - \sqrt{\left(\frac{A}{B}\right)^2 + 4\frac{k_x}{B}} \right) < 0.$$

Recall $\alpha^2 = -B$. The modular parameter m and frequency $\tilde{\alpha}$ are given by:

$$m = \frac{e^2 + d^2}{e^2}, \quad (\text{A.28})$$

$$\tilde{\alpha}^2 = \alpha^2 e^2 = -Be^2. \quad (\text{A.29})$$

Special Limit: Soliton Solution ($m \rightarrow 1$)

As the modular parameter $m \rightarrow 1$, the Jacobian elliptic functions degenerate to hyperbolic functions:

$$\text{cn}(z, 1) = \text{sech}(z), \quad \text{sn}(z, 1) = \tanh(z).$$

For $m \rightarrow 1$, we have $e^2 - d^2 \rightarrow e^2$ (i.e., $d^2 \rightarrow 0$), which eliminates the constant term in Ψ . Substituting into Eq. (A.21), the periodic solution reduces to the localized soliton solution (valid for $y \in \mathbb{R}$, decaying to 0 as $y \rightarrow \pm\infty$):

$$\Phi(y) = \sqrt{e^2 [1 - 1 \cdot \text{sn}^2(\tilde{\alpha}y, 1)]} = \sqrt{e^2 [1 - \tanh^2(\tilde{\alpha}y)]} = e \cdot \text{sech}(\tilde{\alpha}y). \quad (\text{A.30})$$

This soliton solution satisfies the key physical property of localization: $\Phi(y) \rightarrow 0$ as $y \rightarrow \pm\infty$, consistent with the normalization condition $\int_{-\infty}^{\infty} \Phi^2(y) dy = 1$.

References

- [1] EN Tsoy, A Ankiewicz, and N Akhmediev. Dynamical models for dissipative localized waves of the complex ginzburg-landau equation. *PHYSICAL REVIEW E*, 73(3, 2), MAR 2006. ISSN 2470-0045. doi: 10.1103/PhysRevE.73.036621.
- [2] Orazio Descalzi, M. Facão, M.I. Carvalho, Carlos Cartes, and Helmut R. Brand. Dissipative pulses stabilized by nonlinear gradient terms: A review of their dynamics and their interaction. *Physica D: Nonlinear Phenomena*, 473:134520, 2025. ISSN 0167-2789. doi: <https://doi.org/10.1016/j.physd.2024.134520>. URL <https://www.sciencedirect.com/science/article/pii/S0167278924004706>.
- [3] Wolfgang Schöpf and Walter Zimmermann. Convection in binary fluids: Amplitude equations, codimension-2 bifurcation, and thermal fluctuations. *Phys. Rev. E*, 47:1739–1764, Mar 1993. doi: 10.1103/PhysRevE.47.1739. URL <https://link.aps.org/doi/10.1103/PhysRevE.47.1739>.
- [4] A H Khater, D K Callebaut, and A R Seadawy. General soliton solutions for nonlinear dispersive waves in convective type instabilities. *Physica Scripta*, 74(3):384, aug 2006. doi: 10.1088/0031-8949/74/3/015. URL <https://doi.org/10.1088/0031-8949/74/3/015>.
- [5] Boris A. Malomed. Optical solitons and vortices in fractional media: A mini-review of recent results. *PHOTONICS*, 8(9), SEP 2021. doi: 10.3390/photonics8090353.
- [6] M. C. Cross and P. C. Hohenberg. Pattern formation outside of equilibrium. *Rev. Mod. Phys.*, 65:851–1112, Jul 1993. doi: 10.1103/RevModPhys.65.851. URL <https://link.aps.org/doi/10.1103/RevModPhys.65.851>.

[7] Igor S. Aranson and Lorenz Kramer. The world of the complex ginzburg-landau equation. *Rev. Mod. Phys.*, 74:99–143, Feb 2002. doi: 10.1103/RevModPhys.74.99. URL <https://link.aps.org/doi/10.1103/RevModPhys.74.99>.

[8] Maria Blum, Christian Döding, and Patrick Henning. Vortex-capturing multiscale spaces for the ginzburg–landau equation. *Multiscale Modeling & Simulation*, 23(1):339–373, 2025. doi: 10.1137/24M1664538. URL <https://doi.org/10.1137/24M1664538>.

[9] Robert W. Richardson. Ginzburg-landau theory of anisotropic superfluid neutron-star matter. *Physical Review D*, 5:1883–1896, 1972. URL <https://api.semanticscholar.org/CorpusID:120735026>.

[10] Emmanuel Kengne, Wu-Ming Liu, Lars Q. English, and Boris A. Malomed. Ginzburg–landau models of nonlinear electric transmission networks. *Physics Reports*, 982:1–124, 2022. ISSN 0370-1573. doi: <https://doi.org/10.1016/j.physrep.2022.07.004>. URL <https://www.sciencedirect.com/science/article/pii/S037015732200268X>. Ginzburg-Landau models of nonlinear electric transmission networks.

[11] J. D. Scheel, M. R. Paul, M. C. Cross, and P. F. Fischer. Traveling waves in rotating rayleigh-bénard convection: Analysis of modes and mean flow. *Phys. Rev. E*, 68:066216, Dec 2003. doi: 10.1103/PhysRevE.68.066216. URL <https://link.aps.org/doi/10.1103/PhysRevE.68.066216>.

[12] Emmanuel Yomba and Poonam Ramchandra Nair. New coupled optical solitons to birefringent fibers for complex ginzburg-landau equations with hamiltonian perturbations and kerr law nonlinearity. *MATHEMATICS*, 12(19), OCT 2024. doi: 10.3390/math12193073.

[13] Sachin Kumar, Saurabh Kumar Sharma, Ravi Karwasra, Sandeep Malik, Taher A. Nofal, and Ahmed H. Arnous. Soliton structures, bifurcation patterns, and chaos in a nonlinear transmission line governed by the modified complex ginzburg–landau equation. *Chaos, Solitons & Fractals*, 200:117068, 2025. ISSN 0960-0779. doi: <https://doi.org/10.1016/j.chaos.2025.117068>.

org/10.1016/j.chaos.2025.117068. URL <https://www.sciencedirect.com/science/article/pii/S0960077925010811>.

[14] R. B. Hoyle. Zigzag and Eckhaus instabilities in a quintic-order nonvariational ginzburg-landau equation. *Phys. Rev. E*, 58:7315–7318, Dec 1998. doi: 10.1103/PhysRevE.58.7315. URL <https://link.aps.org/doi/10.1103/PhysRevE.58.7315>.

[15] Robert A. Van Gorder. Complex ginzburg–landau equation for time-varying anisotropic media. *Studies in Applied Mathematics*, 153(3):e12730, 2024. doi: <https://doi.org/10.1111/sapm.12730>. URL <https://onlinelibrary.wiley.com/doi/abs/10.1111/sapm.12730>.

[16] N. N. Akhmediev, A. Ankiewicz, and J. M. Soto-Crespo. Multisoliton solutions of the complex ginzburg-landau equation. *Phys. Rev. Lett.*, 79:4047–4051, Nov 1997. doi: 10.1103/PhysRevLett.79.4047. URL <https://link.aps.org/doi/10.1103/PhysRevLett.79.4047>.

[17] Hadi Rezazadeh. New solitons solutions of the complex ginzburg-landau equation with kerr law nonlinearity. *OPTIK*, 167:218–227, 2018. ISSN 0030-4026. doi: 10.1016/j.ijleo.2018.04.026.

[18] N Akhmediev, JM Soto-Crespo, and G Town. Pulsating solitons, chaotic solitons, period doubling, and pulse coexistence in mode-locked lasers: Complex ginzburg-landau equation approach - art. no. 056602. *PHYSICAL REVIEW E*, 63(5, 2), MAY 2001. ISSN 2470-0045. doi: 10.1103/PhysRevE.63.056602.

[19] N Akhmediev and VV Afanasjev. Novel arbitrary-amplitude soliton solutions of the cubic-quintic complex ginzburg-landau equation. *Phys Rev Lett*, 75(12):2320–2323, Sep 1995. ISSN 1079-7114 (Electronic); 0031-9007 (Linking). doi: 10.1103/PhysRevLett.75.2320.

[20] R. Montagne, E. Hernández-García, and M. San Miguel. Numerical study of a lyapunov functional for the complex ginzburg-landau equation. *Physica D: Nonlin-*

ear Phenomena, 96(1):47–65, 1996. ISSN 0167-2789. doi: [https://doi.org/10.1016/0167-2789\(96\)00013-9](https://doi.org/10.1016/0167-2789(96)00013-9). URL <https://www.sciencedirect.com/science/article/pii/0167278996000139>.

[21] Stefan C. Mancas and S. Roy Choudhury. Traveling wavetrains in the complex cubic–quintic ginzburg–landau equation. *Chaos, Solitons & Fractals*, 28(3):834–843, 2006. ISSN 0960-0779. doi: <https://doi.org/10.1016/j.chaos.2005.08.080>. URL <https://www.sciencedirect.com/science/article/pii/S0960077905006351>.

[22] R. Abraham and J.E. Marsden. *Foundations of Mechanics*. Benjamin/Cummings Publishing Co., Reading, MA, USA, 1978. ISBN 0-8053-0102-X.

[23] Mikio Nakahara. *Geometry, Topology and Physics*. CRC Press, New York, 10 2018. ISBN 9781315275826. doi: <https://doi.org/10.1201/9781315275826>.

[24] Alessandro Bravetti, Hans Cruz, and Diego Tapias. Contact Hamiltonian Mechanics. *Annals of Physics*, 376:17–39, 1 2017. ISSN 0003-4916. doi: <https://doi.org/10.1016/j.aop.2016.11.003>.

[25] De Yu Zhong and Guang Qian Wang. Kinetic Equation for Stochastic Vector Bundles. *Journal of Physics A: Mathematical and Theoretical*, 57(22):225004, 5 2024. doi: <https://doi.org/10.1088/1751-8121/ad483a>.

[26] Jordi Gaset, Xavier Gràcia, Miguel C. Muñoz Lecanda, Xavier Rivas, and Narciso Román-Roy. New contributions to the hamiltonian and lagrangian contact formalisms for dissipative mechanical systems and their symmetries. *International Journal of Geometric Methods in Modern Physics*, 17(06):2050090, 2020. doi: 10.1142/S0219887820500905. URL <https://doi.org/10.1142/S0219887820500905>.

[27] Kang-Jia Wang, Hong-Wei Zhu, Shuai Li, Feng Shi, Geng Li, and Xiao-Lian Liu. Bifurcation analysis, chaotic behaviors, variational principle, hamiltonian and diverse optical solitons of the fractional complex ginzburg–landau model. *INTERNATIONAL*

JOURNAL OF THEORETICAL PHYSICS, 64(5), MAY 7 2025. ISSN 0020-7748. doi: 10.1007/s10773-025-05977-9.

- [28] V. I. Arnold. *Contact Geometry and Wave Propagation: Lectures Given at the University of Oxford under the Sponsorship of the International Mathematical Union*. L'Enseignement mathématique, Université de Genève, Genève, 1989. URL <https://iucat.iu.edu/iub/86833>.
- [29] Hansjörg Geiges. *An Introduction to Contact Topology*, volume 109 of *Cambridge Studies in Advanced Mathematics*. Cambridge University Press, London, 2008. doi: <https://doi.org/10.1017/CBO9780511611438>.
- [30] D.Y. Zhong and G.Q. Wang. Least constraint and contact dynamics of stochastic vector bundles. *Chaos, Solitons and Fractals*, 201:117143, 2025. ISSN 0960-0779. doi: <https://doi.org/10.1016/j.chaos.2025.117143>. URL <https://www.sciencedirect.com/science/article/pii/S0960077925011567>.
- [31] Alan C. Newell and J. A. Whitehead. Finite bandwidth, finite amplitude convection. *Journal of Fluid Mechanics*, 38(2):279–303, 1969. doi: 10.1017/S0022112069000176.
- [32] Lee A. Segel. Distant side-walls cause slow amplitude modulation of cellular convection. *Journal of Fluid Mechanics*, 38(1):203–224, 1969. doi: 10.1017/S0022112069000127.
- [33] Martin Brokate and Jürgen Sprekels. *Phase Transitions and Hysteresis*, pages 150–174. Springer New York, New York, NY, 1996. ISBN 978-1-4612-4048-8. doi: 10.1007/978-1-4612-4048-8_5. URL https://doi.org/10.1007/978-1-4612-4048-8_5.
- [34] Hongbo Jiang, Ruilong Song, Jiayi Shen, Zhiming Yang, Yuantong Liu, Xinxu Duan, Xiaoyun Tang, and Lei Jin. Transitions between periodic waves and soliton states in a polarization-dependent loss-tailored fiber laser. *Optics & Laser Technology*, 192:113838, 2025. ISSN 0030-3992. doi: <https://doi.org/10.1016/j.optlastec.2025.113838>. URL <https://www.sciencedirect.com/science/article/pii/S003039922501429X>.